skb.se

SKB R-25-12

ISSN 1402-3091
ID 2091620
December 2025

Comparison of numerical methods for determining the dilution of repository-depth groundwater at Forsmark

David Applegate
Amentum

Steve Joyce
MCM Environmental Services Ltd.

Jan-Olof Selroos
Svensk Kärnbränslehantering AB

Keywords: DFN, dilution, Forsmark, salinity.

Summary

Forsmark is the proposed site for a repository providing long-term disposal of spent fuel from Swedish nuclear power reactors. It is envisaged that spent fuel will be disposed of in vertically placed copper canisters, surrounded by bentonite, at a depth of approximately 500 m within a sparsely fractured crystalline bedrock at the Forsmark site. The salinity of the groundwater around the repository is a key parameter affecting the post-closure performance of the disposal system, as it influences the performance of the bentonite buffer.

This work presents illustrative simulations of the future evolution of the groundwater composition within the Forsmark repository. These calculations use the Block 1 repository-scale mesh from SR-Site and a plane-projected representation of the deformation zones. Holocene climatic conditions and present-day sea levels are assumed to persist for the duration of the calculations.

The key aspect and motivation for this work is that three separate simulation techniques have been compared:

- Equivalent continuous porous media (ECPM) simulations of saline transport using the advection-diffusion equations (ADE) with and without rock matrix diffusion (RMD).
- Discrete fracture network (DFN) ADE simulations of saline transport, with and without RMD.
- DFN based advective particle tracking simulations. These calculations include variants with and without an analytical representation of rock matrix diffusion.

Salinity transport calculations involving mixing between saline and dilute reference waters show qualitative agreement between the ECPM ADE, DFN ADE and DFN pathline calculations. All show dilution increasing with time at repository depth, with the ECPM and pathline-based calculations predicting faster dilution than the DFN ADE calculations. The ADE-based methods also indicate that some locations may experience transient increases in salinity due to flow paths descending below repository depth, a behaviour not captured by pathline approaches that assume constant salinity.

Calculations with five reference waters have also been carried out, analogous to those performed for SR-Site but on a repository scale. These calculations include coupled flow and transport and enable the prediction of the evolution of full groundwater composition, rather than salinity alone. They are not comparable to the calculations with two reference waters, due to the use of different boundary conditions. Overall, the ECPM and DFN calculations with five reference waters exhibit similar behaviour, as the fraction of meteoric water clearly increases over time at repository depth. However, there are some localised differences likely due to changes in connectivity brought about by the upscaling process.

This study also highlights the trade-offs associated with each modelling approach. The pathline method is highly tractable and includes many relevant physical processes but does not explicitly represent dispersion or spatially varying initial conditions. ECPM methods improve on these points but lack structural realism of the DFN approach and tend to overestimate mixing. The DFN ADE approach, though more computationally demanding, provides a geologically realistic framework for solute transport and explicitly includes dispersion and the variable initial distribution of salinity.

Recommendations for future work include extending the DFN simulation domain to incorporate all main recharge locations. Combined DFN-ECPM models would be an effective means of doing this, currently under development within ConnectFlow. Other options may include considering whether simulations with five-reference waters are required for salinity-focused assessments, and further development of pathline methods to allow spatially variable initial conditions. Including chemical reactions would remove a source of conservatism within the DFN ADE calculations.

Finally, this work has focused on comparing different methodologies for calculating dilution and it was therefore deemed unnecessary to consider uncertainty within the fracture network. This uncertainty would likely need to be considered in a formal assessment, potentially by generating and simulating dilution for a range of different fracture realisations.

Sammanfattning

Forsmark är den föreslagna platsen för ett slutförvar för långsiktig deponering av använt kärnbränsle från svenska kärnkraftsreaktorer. Det är tänkt att det använda bränslet ska deponeras i vertikalt placerade kopparkapslar, omgivna av bentonit, på ett djup av cirka 500 meter i gles sprickig kristallin berggrund vid Forsmark. Salthalten i grundvattnet kring förvaret är en nyckelparameter som påverkar förvarets funktion efter förslutning, eftersom den påverkar bentonitbuffertens egenskaper.

Detta arbete presenterar illustrativa simuleringar av den framtida utvecklingen av grundvattnets sammansättning inom Forsmarks förvar. Beräkningarna använder Block 1 av modellen på förvarsskala från SR-Site, samt en planprojektion av deformationszonerna. Holocena klimatförhållanden och dagens havsnivåer antas bestå under hela beräkningsperioden.

Den centrala aspekten och motivet för detta arbete är att tre separata simuleringstekniker har jämförts:

- ECPM (Equivalent Continuous Porous Media) simuleringar av salttransport med advektions-diffusionsekvationen (ADE), med och utan matrisdiffusion (RMD).
- DFN (Discrete Fracture Network) ADE-simuleringar av salttransport, med och utan RMD.
- DFN-baserade advektiva partikelspårningssimuleringar, inklusive varianter med och utan en analytisk representation av matrisdiffusion.

Beräkningar av salttransport som involverar blandning mellan salta och utspädda referensvatten visar en kvalitativ överensstämmelse mellan ECPM ADE, DFN ADE och DFN-partikelspårningsberäkningar. Alla metoder visar att utspädningen ökar med tiden på förvarsdjup, där ECPM- och de partikelspårningsbaserade beräkningarna predikterar snabbare utspädning än DFN ADE-beräkningarna. De ADE-baserade metoderna indikerar också att vissa platser kan erhålla tillfälliga ökningar i salthalt på grund av flödesvägar som går under förvarsdjupet – ett beteende som inte fångas av partikelspårningsmetoder som antar konstant salthalt.

Beräkningar med fem referensvatten har också genomförts, analogt med de som gjordes för SR-Site men i förvarsskala. Dessa beräkningar inkluderar kopplade flödes- och transportberäkningar och möjliggör prediktioner av den fullständiga utvecklingen av grundvattnets sammansättning, snarare än av enbart salthalt. De är inte jämförbara med beräkningarna med två referensvatten eftersom olika randvillkor använts. Sammantaget uppvisar ECPM- och DFN-beräkningarna med fem referensvatten liknande beteende, där andelen meteoriskt vatten tydligt ökar över tid på förvarsdjup. Dock finns vissa lokala skillnader, sannolikt beroende på förändringar i konnektivitet som uppstår genom uppskalningsprocessen.

Studien belyser också de begränsningar som är förknippade med varje modelleringsmetod. Partikelspårningsmetoden är mycket lätthanterlig och inkluderar många relevanta fysikaliska processer men representerar inte explicit dispersion eller rumsligt varierande initialvillkor. ECPM-metoden förbättrar dessa aspekter men saknar den strukturella realism som DFN-metoden erbjuder och tenderar att överskatta blandning. DFN ADE-metoden, även om den är mer beräkningskrävande, erbjuder en geologiskt realistisk ram för ämnestransport och inkluderar explicit dispersion samt den variabla initiala fördelningen av salthalt.

Rekommendationer för framtida arbete inkluderar att utvidga DFN-simuleringsdomänen till att omfatta alla huvudsakliga tillrinningsområden. Kombinerade DFN-ECPM-modeller skulle vara ett effektivt sätt att göra detta och är för närvarande under utveckling inom ConnectFlow. Andra alternativ kan vara att överväga om simuleringar med fem referensvatten behövs för bedömning av salthalt, samt vidareutveckling av partikelspårningsmetoder för att tillåta rumsligt varierande initialvillkor. Att inkludera kemiska reaktioner skulle ta bort en källa till konservatism inom DFN ADE-beräkningarna.

Slutligen har detta arbete fokuserat på att jämföra olika metoder för beräkning av utspädning och det ansågs därför onödigt att beakta osäkerhet inom spricknätverket. Denna osäkerhet skulle sannolikt behöva beaktas i en formell analys, eventuellt genom att generera och simulera utspädning för en rad olika sprickrealiseringar.

Acknowledgements

The authors are very grateful to Dr. Pirouz Shahkarami at Kemakta Konsult AB for the analytical post-processing of particle tracking calculations to include the effect of rock matrix diffusion. We are also grateful to Dr. Thomas Williams, Dr. Guanqun Gai and Dr. Russell Niven, who made key contributions to the early stages of ConnectFlow modelling.

Content

1 Introduction 5

2 Previous work on dilution of repository porewater 6
2.1 Overview of work carried out for SR-Site 6
2.1.1 Overview of SR-Site 6
2.1.2 Forsmark site overview 6
2.1.3 SR-Site conceptual model 6
2.1.4 SR-Site numerical models 11
2.1.5 Future evolution of groundwater composition 15
2.1.6 Previous calculations of dilute water penetration at Forsmark 16
2.2 More recent work 18
2.2.1 Longer-term hydrogeochemical evolution at Forsmark 18
2.2.2 Further calculations of dilute water penetration at Forsmark 21
2.2.3 Dilution of groundwater at Olkiluoto 23

3 Modelling solute transport using DFNs 26
3.1 DFN flow and transport equations 26
3.2 Numerical approach and discretisation 27
3.3 Rock matrix diffusion 27
3.4 Reference waters 29

4 Model description 30
4.1 Model Domain 30
4.2 Fracture System 31
4.3 Groundwater composition 33
4.4 Rock properties 34
4.5 Initial conditions and boundary conditions 34
4.6 Upscaling 36
4.7 Particle tracking and analytic RMD calculations 36

5 Calculation Results for two reference waters 39
5.1 Comparison of advective pathlines with advection-dispersion calculations without RMD 39
5.2 Comparison of advective pathlines with advection-dispersion calculations using RMD 42
5.3 The impact of coupling flow and salinity 45
5.4 Comparisons at specific locations 45

6 Five reference water calculations 48

7 Conclusions 55

8 Significance and Recommendations for Future Work 57

9 References 58

1 Introduction

Forsmark is the proposed site for the long-term disposal of spent fuel from Swedish nuclear power reactors. The KBS-3V disposal system, developed by SKB, envisages that spent fuel will be disposed of in vertically placed copper canisters, surrounded by bentonite, at a depth of approximately 500 m within a sparsely fractured crystalline bedrock at the Forsmark site.

The salinity of the groundwater around the repository is a key parameter affecting the post-closure performance of the KBS-3V disposal system. This impacts the performance of the bentonite buffer. SKB's preliminary safety assessment report (PSAR) states (SKB 2022a) that low salinities can erode the bentonite buffer. The present-day salinity of the repository groundwater at Forsmark is moderate, at around 10 g/L (Joyce et al. 2010a). This salinity is expected to decrease due to the infiltration of meteoric water which may eventually penetrate to repository depth and dilute the groundwater around the repository. Thus, there is significant interest in determining if, when and where dilution to a safety impacting value might occur.

This report summarises previous work concerning the dilution of repository groundwater via meteoric infiltration, with a specific focus on SR-Site (a key source of data for the current work), but also including more recent work from both Forsmark and Olkiluoto in Finland. These previous calculations predict the proportion of deposition holes that would experience a specified degree of dilution after a specified period of time.

These earlier investigations employed two main modelling approaches: pathline-based approaches which include analytical models to include the effect of diffusion into a finite matrix, and/or advection-dispersion calculations carried out using equivalent continuous porous medium (ECPM) representations of the fractured host rock. Those approaches each had strengths and limitations. The pathline-based methods used an explicit representation of the fractures, and in some cases included the impact of stagnant zones, but did not explicitly capture dispersion processes (instead using ensembles of pathlines to capture the effect of dispersion) and did not consider the initial variation in the salinity distribution within the fractures and matrix. ECPM based calculations removed most of those limitations but tended to overestimate mixing and dispersion and do not explicitly represent individual fractures or their intersections - features that strongly influence solute migration in crystalline rock.

Building on this foundation, the current work introduces a new approach where the advection-diffusion equations are solved within a discrete fracture network (DFN), allowing for a more detailed and geologically realistic treatment of flow and transport. Recent improvements to the ConnectFlow software (Applegate and Appleyard 2022), have made such DFN-based modelling feasible at repository scale.

The primary objective of this study is to simulate the evolution of groundwater salinity within the Forsmark repository under temperate climatic conditions using a repository scale simulation domain. These illustrative calculations compare explicit DFN-based advection-dispersion simulations with results from an ECPM model to assess the limitations of the ECPM approach. Additionally, advective DFN pathline calculations incorporating an analytical treatment of rock matrix diffusion are used as a further comparison to understand the significance of the approximations made in that approach.

Section 2 of this report details previous work considering dilution of repository water, with specific focus on SR-Site; Section 3 describes the ConnectFlow approach to saline transport within fracture networks; Section 4 describes the three different models that have been used to represent transport at Forsmark in this report; Section 5 presents the results of these calculations assuming a simplified mixture of dilute and saline water; Section 6 includes variant calculations with a more complex mixture of ancient brine (deep saline), Littorina sea water, meteoric, glacial and old meteoric water; Section 7 summarises the main conclusions; finally, Section 8 discusses the significance of the conclusions and recommends further work.

2 Previous work on dilution of repository porewater

2.1 Overview of work carried out for SR-Site

2.1.1 Overview of SR-Site

SR-Site was an SKB project to assess the long-term safety of a final repository for spent nuclear fuel, to be located at Forsmark in Sweden (SKB 2011). The project supported SKB's license application for the construction and operation of the repository, submitted in 2011.

SR-Site was underpinned by decades of research, site investigations, site characterisation, modelling work and expert evaluation. The site-description of Forsmark compiled during the site investigation is presented in SKB (2008). Further reports consider various topics in more detail, for example, the bedrock hydrogeology is presented in Follin (2008), while details of the regolith are considered in Hedenström et al. (2008). The original strategy for the site investigations at Forsmark was presented in Rhén et al. (2003).

SR-Site considered and assessed many aspects of the long-term safety of a repository at Forsmark. Those of relevance to the current work are concerned with the hydrogeological and hydrogeochemical evolution within the bedrock at Forsmark and are summarised in the following sections. In particular, the potential for dilute groundwater to reach deposition hole locations is explored. This is of potential concern as a significant reduction in the salinity of the groundwater can lead to erosion of the bentonite buffer in deposition holes.

2.1.2 Forsmark site overview

The intended site for the Swedish spent nuclear fuel repository lies below relatively flat coastal land at Forsmark on the edge of the Baltic Sea, approximately 120 km north of Stockholm. The bedrock is largely granitic crystalline rock overlain by relatively thin quaternary deposits. The bedrock has been subject to both ductile and brittle deformation. The repository location lies within a very sparsely fractured tectonic lens, which has been less affected by ductile deformation, enclosed by ductile high strain belts.

The Forsmark area is (currently) subject to post-glacial land rise of around 6 mm per year. The coastal location and fairly flat topography lead to continuous transformation of marine areas into new terrestrial areas or lakes (Figure 2), with lakes and wetlands being successively covered by peat. The rate of land rise is expected to reduce in the future, with the effects being further reduced due to global sea level rise because of climate change.

2.1.3 SR-Site conceptual model

The hydrogeological conceptual model used for SR-Site was defined in terms of three domains (illustrated in Figure 2-3):

- The Hydraulic Conductor Domain (HCD): The deformation zones;
- The Hydraulic Rock mass Domain (HRD): The less fractured bedrock between the deformation zones;
- The Hydraulic Soil Domain (HSD): The regolith (Quaternary deposits) lying above the bedrock.

The bedrock domains have been extensively characterised, primarily by borehole investigations, which included hydraulic testing and groundwater sampling.

The deformation zones within the HCD represent bands of enhanced fracturing (relative to the surrounding bedrock). They range from steeply dipping to gently dipping and show a strong depth trend in transmissivity, with the transmissivity decreasing with increasing depth. The hydraulic properties including transmissivity also differ between the various deformation zones.

Towards the top of the bedrock are a series of sub-horizontal sheet joints (shown in Figure 2-4), that are laterally extensive and can be highly transmissive. They play an important role in the movement of groundwater in the upper bedrock, as illustrated schematically in Figure 2-5.

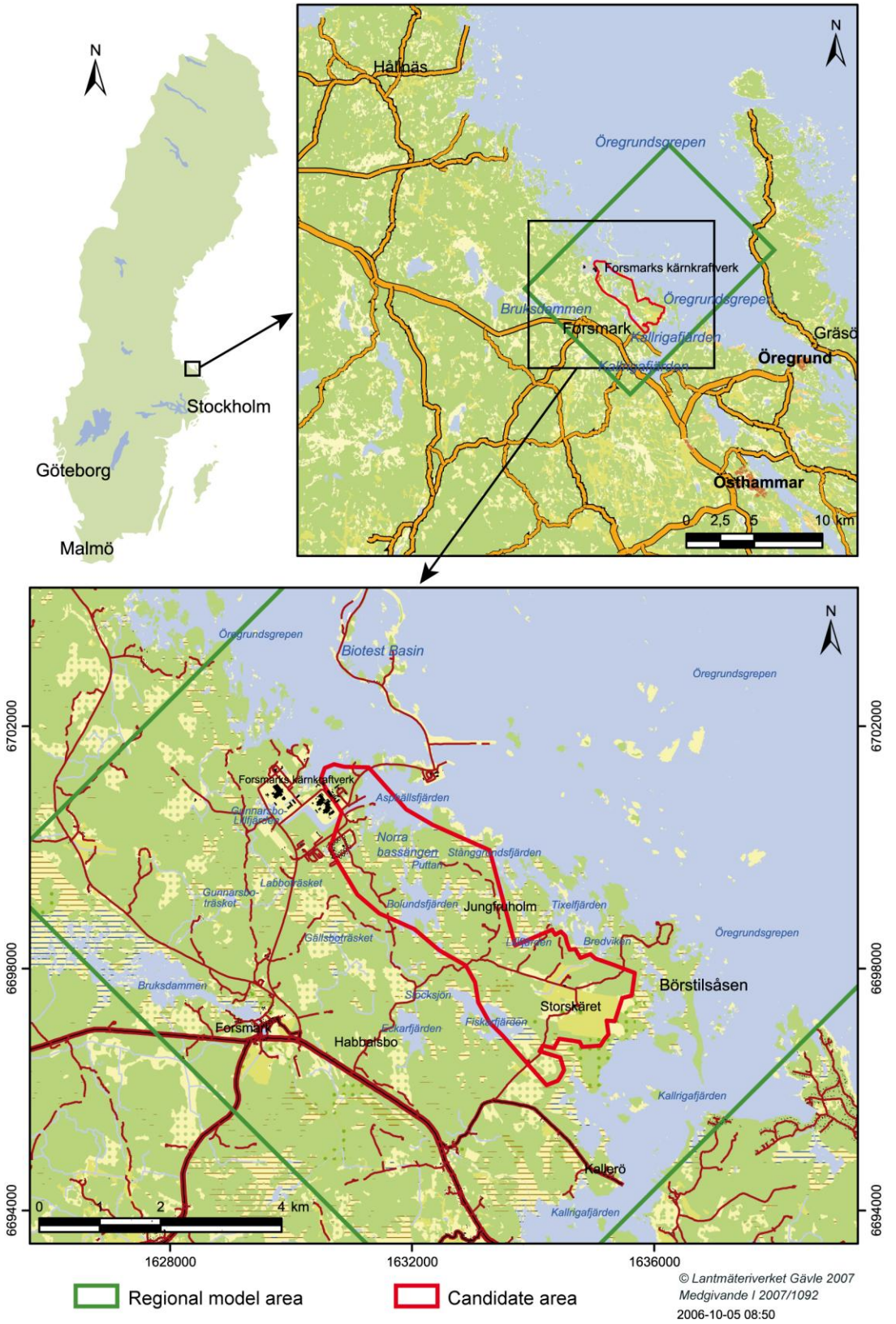

Figure 2-1. *The location of the Forsmark site (Figure 1-3 in SKB 2008).*

Figure 2-2. *The flat topography and the low-gradient shoreline at Forsmark with recently isolated bays due to land uplift (Figure 1-7 in Follin 2008).*

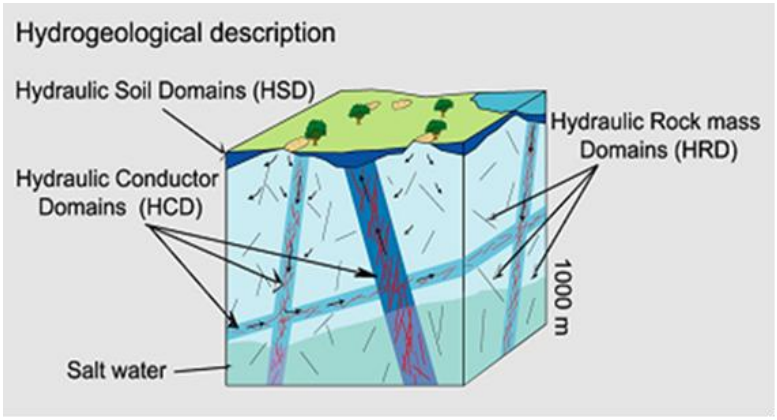

Figure 2-3. *Illustration of the domains (HCD, HRD, HCD) within the SR-Site conceptual hydrogeological model (Figure 3-2 in Rhén et al. 2003).*

The fractured rock between the deformation zones forming the HRD has been subdivided into fracture domains (FFM01 to FFM06) based on location and the characteristics of the fracturing (Figure 2-6). Within these domains five fracture orientation sets were identified according to observed groupings: North-South trending (NS), Northeast-Southwest trending (NE), Northwest-Southeast trending (NW), East-West trending (EW) and horizontal fractures (HZ). The intensity of fracturing within the HRD also has a depth dependence, which has been represented in the conceptual model by three depth zones (above 200 m, 200 m to 400 m and below 400 m depth); fracture intensity typically decreases with depth. (Note that the models used more than fifty fracture "sets" to facilitate the grouping fractures according to depth, orientation and domain, these are distinct from the five formal fracture orientation sets previously described).

The Quaternary deposits comprising the regolith form layers of varying composition across the site. The total thickness of the HSD ranges from a few decimetres up to 42 m (Figure 2-7). In most places, the thickness is a few metres or less. The Quaternary deposits have been conceptualised within the HSD as a set of nine layers, as shown in Figure 2-8. Note that not all HSD layers are present across the whole model domain.

Figure 2-4. *Sheet joints visible in the sides of the canal between the Baltic Sea and the nuclear power plant at Forsmark (Figure 5-14 in Follin 2008).*

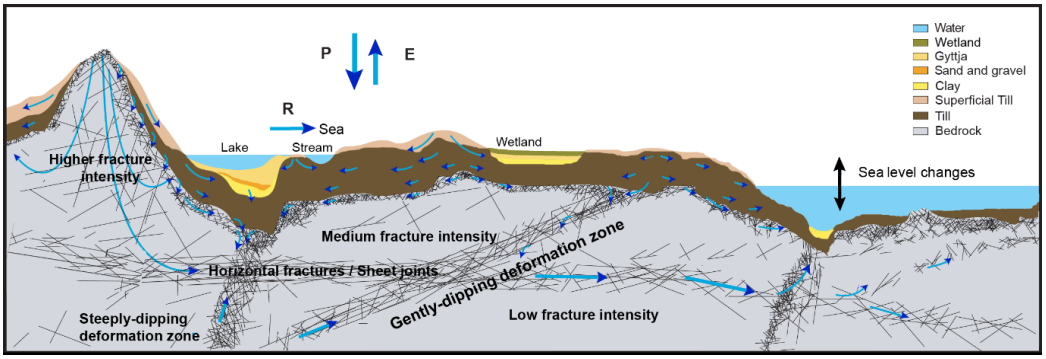

Figure 2-5. *A (vertically exaggerated) cross-section illustrating the movement of groundwater in the shallow bedrock aquifer (Figure 5-16 in Follin 2008).*

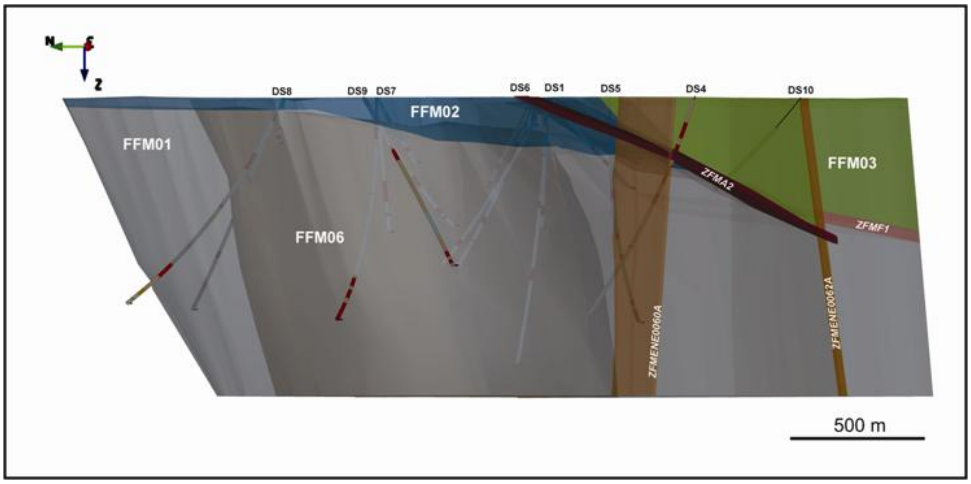

Figure 2-6. *Representation of the Forsmark fracture domain model. Some deformation zones and boreholes are also shown. (Figure 3-10 in Follin 2008).*

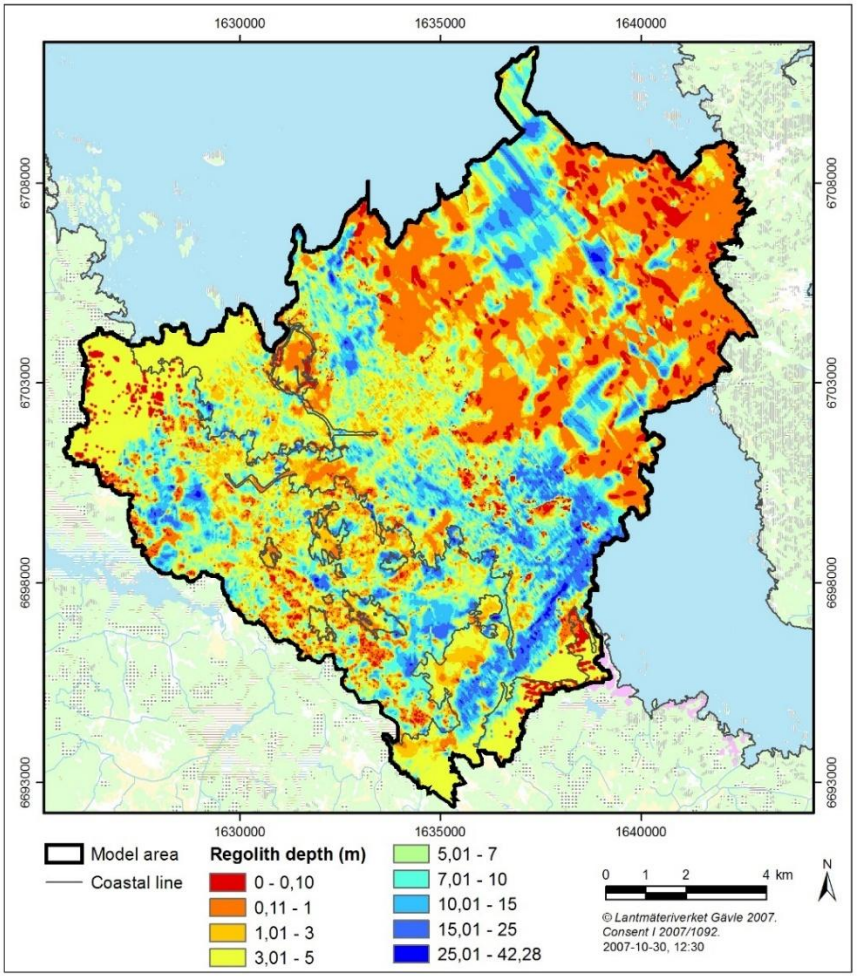

Figure 2-7. *Interpreted total thickness of quaternary deposits (from Figures in Appendix 2 of Hedenström et al. 2008).*

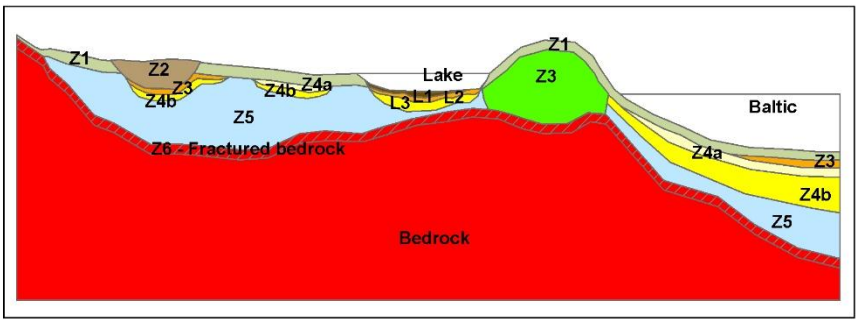

Figure 2-8. *Vertical slice (vertically exaggerated) of the conceptual model for the HSD (Figure 3-1 in Hedenström et al. 2008). Z1 is a surface layer (for example soil); Z2 is peat; Z3 is postglacial sand/gravel, glaciofluvial sediment and artificial fill; Z4a is postglacial clay including gyttja clay; Z4b is glacial clay; Z5 is Till; Z6 is fractured bedrock. There are 3 separate lacustrine lenses; L1 is Gyttja (algal gyttja, calcareous gyttja, clay gyttja-gyttja clay) and Peat; L2 is postglacial sand and/or gravel; L3 is clay (glacial and postglacial).*

Within the bedrock at Forsmark, the relatively high fracture intensity and higher transmissivities in the deformation zones at shallower depths lead to groundwater circulation that is predominantly restricted to the upper bedrock. Groundwater flow at greater depths is much slower and tends to be focussed in the more conductive deformation zones. As a result, the groundwater in the upper bedrock is much more responsive to changes in surface conditions, e.g. due to climate, whereas conditions evolve more slowly at depth. The changes in flow rates with depth affects the penetration of dilute groundwater to repository depth considered within this report.

2.1.4 SR-Site numerical models

The models used for groundwater flow and transport modelling as part of SR-Site were implemented at three different scales (shown in Figure 2-9). This approach was taken for practical reasons as it was not possible to model very small-scale processes at the level of individual fractures around deposition holes as well as large-scale processes over several kilometres using the computational facilities available at the time. However, the models at each scale shared the same underlying representation of the fractures as a discrete fracture network (DFN) with the properties of the DFN assigned from the interpretation of the data within the Site Descriptive Model (SDM). In some models, either part or all the DFN was upscaled to an Equivalent Continuous Porous Medium (ECPM) representation for computational efficiency, as indicated in Figure 2-9. Data was passed between the models at each scale to maintain consistent boundary conditions and initial conditions (also shown in Figure 2-9).

The activities that were carried out at each modelling scale and the communication between the models is shown in Figure 2-10. The regional-scale model was used to calculate the long-term evolution of groundwater flow and composition (in terms of reference waters), taking account of the evolving landscape and climate conditions. The site-scale and repository-scale models were primarily used to calculate more detailed flows within fractures at snapshots in time using data imported from the regional-scale model at those times. The models at these two scales were also used for particle tracking calculations which were the primary input in the calculation of performance measures for the safety assessment.

Within the DFN representation, the deformation zones were represented as planar features that approximated the size, orientation and position of each deformation zone, as estimated from borehole observations. Properties derived from borehole interpretations were then mapped onto the deformation zones, including the depth trend in transmissivity (Figure 2-11 top). In some cases, heterogeneity in transmissivity of the deformation zones was also represented using stochastic variation (Figure 2-11 bottom).

The DFN representation of the HRD consisted of fractures stochastically generated according to property distributions derived from borehole interpretations and calibrated against hydraulic testing data as part of SDM-Site (Follin 2008). Variants with different degrees of correlation between fracture size and hydraulic properties were considered. Multiple realisations of the HRD fractures (and HCDs when lateral heterogeneity within deformation zones was included) were generated (e.g. Figure 2-12), and they were also upscaled for ECPM representations. Only open and connected fractures were modelled, for efficiency and because only these fractures would facilitate groundwater flow and solute transport within the HRD.

The HSD was implemented in the regional-scale and site-scale models as a stacked set of four parallel layers that followed the surface topography. Each layer had the same thickness. The properties of the layers were interpolated and averaged from parameters provided from SDM-Site surface and near-surface modelling (Bosson et al. 2008).

It was assumed within the models that flow and transport occurs primarily within the fractures of the bedrock. However, rock matrix diffusion was also accounted for when calculating the transport of solutes within the groundwater. The solute transport calculations solved the advection-diffusion equations for a set of five reference waters. These reference waters each represent groundwater of a particular origin, e.g. meteoric water or sea water and has a fixed, defined chemical composition with a corresponding salinity. The groundwater salinity was then determined, based on the relative proportions of each reference water, as these reference waters were transported and mixed over time. As the groundwater salinity evolved, the changing groundwater density and viscosity was updated and fed back into the flow calculations in a coupled approach (for regional-scale modelling). For site and repository scale modelling the groundwater density was obtained by interpolation from the regional scale model. Table 2-1 provides a list of the reference waters considered and their properties.

Table 2-1: The properties of five reference waters used in SR-Site. Each reference water has a defined composition of the key groundwater solutes (chloride, sulphate etc. as described in Salas et al. 2010) which when combined with the calculated concentrations of reference waters, allows the precise chemical composition of the groundwater to be specified. For brevity, only the total dissolved solids are stated here. The composition of the meteoric water is modified to take account of carbonate taken up from the regolith.

Water	Density* [kg·m^{-3}]	Total dissolved solids* [kg·m^{-3}]	Salinity [-]	Viscosity* [kg·m^{-1}·s^{-1}]
Brine (deep saline)	1049.8	75.1	7.15×10^{-2}	1.12×10^{-3}
Littorina Sea water	1006.6	11.9	1.18×10^{-2}	1.02×10^{-3}
Meteoric (modified)	998.96	1.06	1.06×10^{-3}	1.00×10^{-3}
Glacial	998.22	0.00200	2.00×10^{-6}	1.00×10^{-3}
Old meteoric	998.65	0.610	6.10×10^{-4}	1.00×10^{-3}

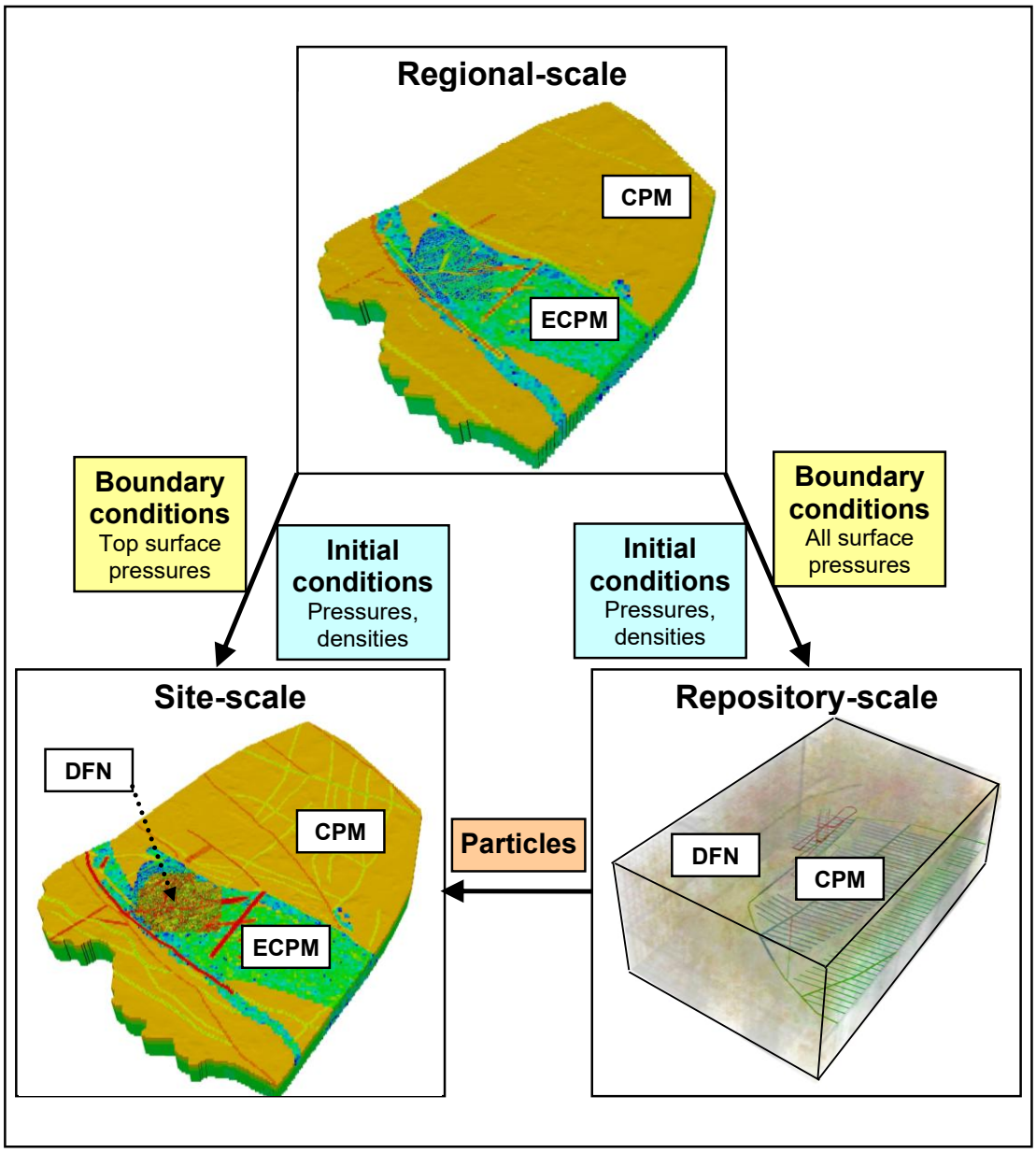

Figure 2-9. *Illustration of model scales, embedding, and the transfer of data between scales for SR-Site. [Figure 3-9 in Joyce et al. (2010a)].*

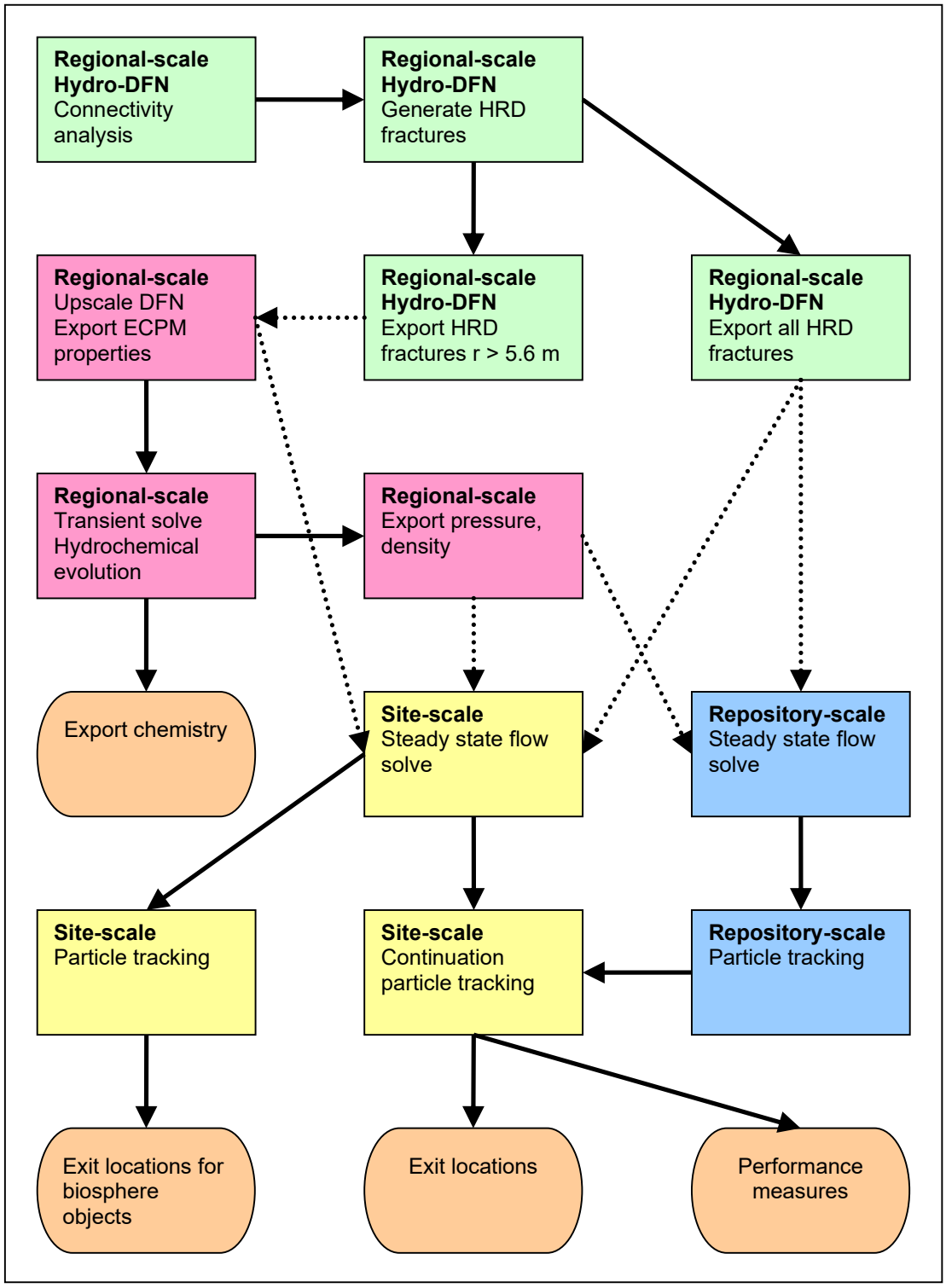

Figure 2-10. *Activities carried out at each modelling scale. Fracture generation is shown in green, regional-scale processes in pink, site-scale processes in yellow and repository-scale processes in blue. Outputs are shown in orange. Solid arrows indicate the modelling workflow within a scale and dotted arrows indicate a transfer of data between scales. While this figure specifies the procedure for exit (discharge locations) a very similar process was followed for recharge locations. [Figure 3-10 in Joyce et al. (2010a)].*

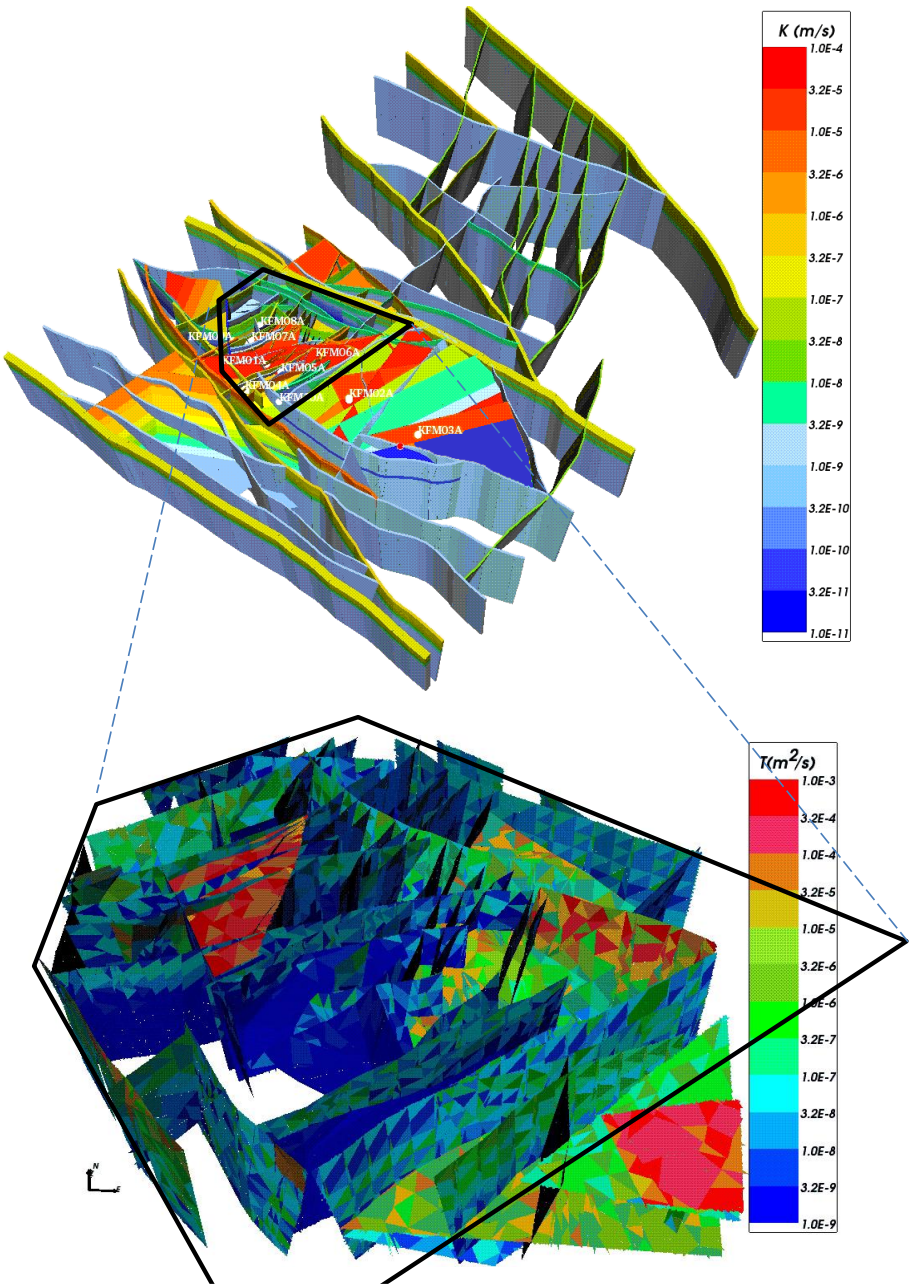

Figure 2-11. *Modelled deformation zones. Top: coloured by hydraulic conductivity showing depth trend. Bottom: Coloured by transmissivity, showing heterogeneity. [Figure 2-5 in Joyce et al. (2010a)].*

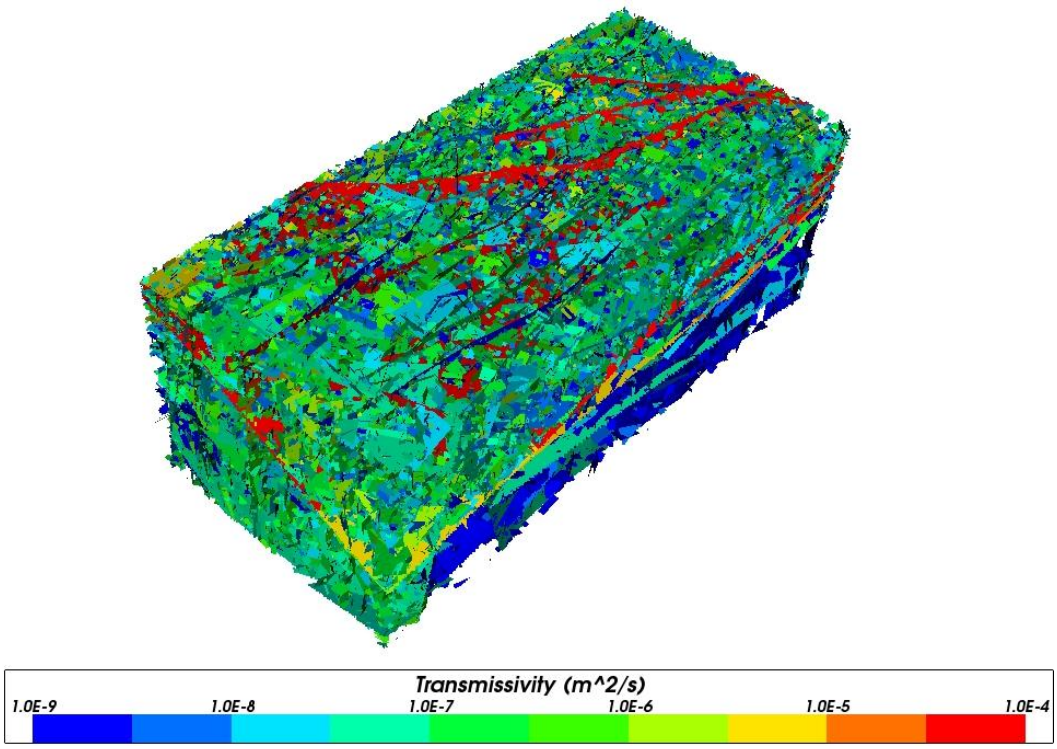

Figure 2-12. *Example repository-scale DFN [Figure 3-1 in Joyce et al. (2010a)].*

2.1.5 Future evolution of groundwater composition

The future evolution of groundwater composition at Forsmark was modelled (in terms of mixing proportions of reference waters) in the regional-scale model by simulating groundwater flow and solute transport from 8,000 BC up to 12,000 AD, representing a single temperate climate period. The simulations started at 8,000 BC because it was possible to estimate a reasonably well-defined initial condition at the end of the last glacial period. The end time of 12,000 AD was taken to correspond to the onset of the next periglacial period according to the climate scenario being used.

The simulations took into account changing boundary conditions due to land rise and changes in infiltrating water composition. Note that groundwater flow at Forsmark is generally towards the coastline, so that as the land rises and the coastline retreats the direction of groundwater flow adjusts accordingly. For the sea bed, infiltrating water through the top surface was assumed to have a time varying salinity, as specified in the SDM (Bosson et al, 2008), to simulate the changing composition of the overlying water. For land areas, infiltration though the top surface water taken to be meteoric water (modified to account for chemical reactions in the near-surface environment). An example of the changes in groundwater composition as a result of the changing groundwater flow patterns and infiltrating water composition is shown in Figure 2-13. These plots illustrate the penetration of meteoric water over the temperate climate period and are indicative of the degree to which dilute water can be transported to repository depth under the simulated conditions. Penetration is slowed in the region around the repository by the sparsity of fractures there.

Additional simulations were also performed that considered groundwater flow and solute transport under glacial conditions using imported boundary conditions from glacial climate period modelling (Vidstrand et al. 2010) for different periods of ice coverage over the Forsmark site.

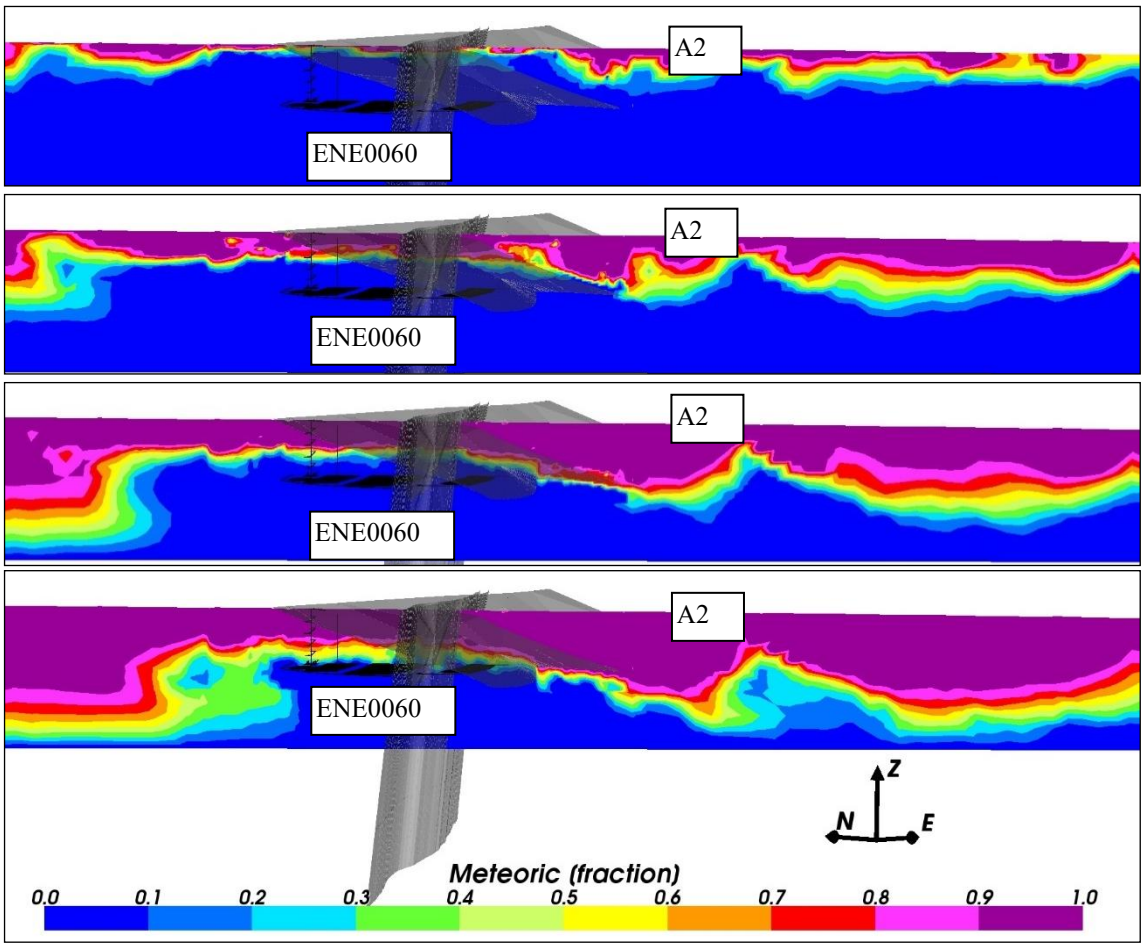

Figure 2-13. *Vertical slices (north west to south east) of the fractional distributions of meteoric water for the regional-scale model. The repository layout and deformation zones A2 and ENE0060 are also shown in black/grey for context. From the top: Distributions at 2000 AD, 3000 AD, 5000 AD and 9000 AD. [Adapted from Figure 6-4 in Joyce et al. 2010a)].*

2.1.6 Previous calculations of dilute water penetration at Forsmark

For SR-Site, an analytical expression was used as part of a particle-based approach to estimate the time taken for dilute water to reach repository depth. This included contributions from advective travel time and retardation due to rock matrix diffusion (Joyce et al. 2010a, Appendix F):

$$t = t_w + \min\left(\frac{F^2 \varepsilon_p D_e}{4\left(\text{erf}^{-1}(\alpha)\right)^2}, \varepsilon_p \delta_m F\right) \qquad (2.1)$$

where t is the dilution time [y], t_w is the advective travel time [y], F is the flow-related transport resistance [y/m], ε_p is the kinematic porosity [-], D_e is the effective diffusivity [m^2/y], δ_m is the average half size of matrix blocks [m] and α is the dilution factor [-] (i.e. the ratio of the current concentration to the initial concentration). This expression incorporates two limiting cases: the first term in the brackets is for an assumption of an infinite-depth matrix and the second term assumes that the transport is slow enough for equilibration between the matrix and fracture. An infinite-depth matrix gives a lower dilution time for lower values of F (below about 3·105 y/m) and an equilibrated matrix gives a lower dilution time for larger values of F, i.e. when advection is sufficiently slow to allow equilibrium with (a finite) rock matrix. More recent work (Poteri et al. 2014, Appendix D) has shown that the value of F that leads to equilibrium occurs when $F \sim L_z/D_e$, where L_z is the matrix depth.

Values of t_w and F at deposition hole locations can be determined by reverse particle tracking, i.e. by releasing particles in fractures intersecting the deposition holes and tracking them back through a reversed groundwater flow field (fixed at a snapshot in time) to the ground surface (e.g. Figure 2-14). The particle tracking was carried out for particular time points during the temperate and glacial climate periods. These results were then used to calculate dilution times at each deposition hole location for particular dilution factors. Of interest were deposition hole locations that might be diluted to the extent that buffer erosion could be a concern (salinity below about 0.3 g/L) within the duration of the climate condition under consideration. Deposition hole locations that were also associated with low t_w and F for transport of radionuclides to the ground surface (determined from forward particle tracking, e.g. Figure 2-14) were of particular interest, as these would be of most concern for post-closure safety.

Figure 2-15 shows the cumulative fraction of deposition hole locations that reach a dilution factor of 0.1 as a function of time. (The dilution factor chosen here is notably conservative because the repository water has an initial salinity of around 10 g/L, and so a dilution factor of 0.1 will result in a salinity of 1 g/L, which is well above the threshold salinity level of 0.3 g/L). There are 52 deposition hole locations that achieve this dilution factor within the 10,000 year temperate period, increasing to 166 locations if the period is extended to 60,000 years (e.g. due to climate warming). Of the 52 deposition hole locations, 11 locations corresponded to F values below 10^5 y/m from forward particle tracking. The low proportion of locations experiencing dilution is largely due to the sparsity of fractures around the repository [it is not explained in Joyce et al. (2010a) how changing the DFN realisation would affect this result].

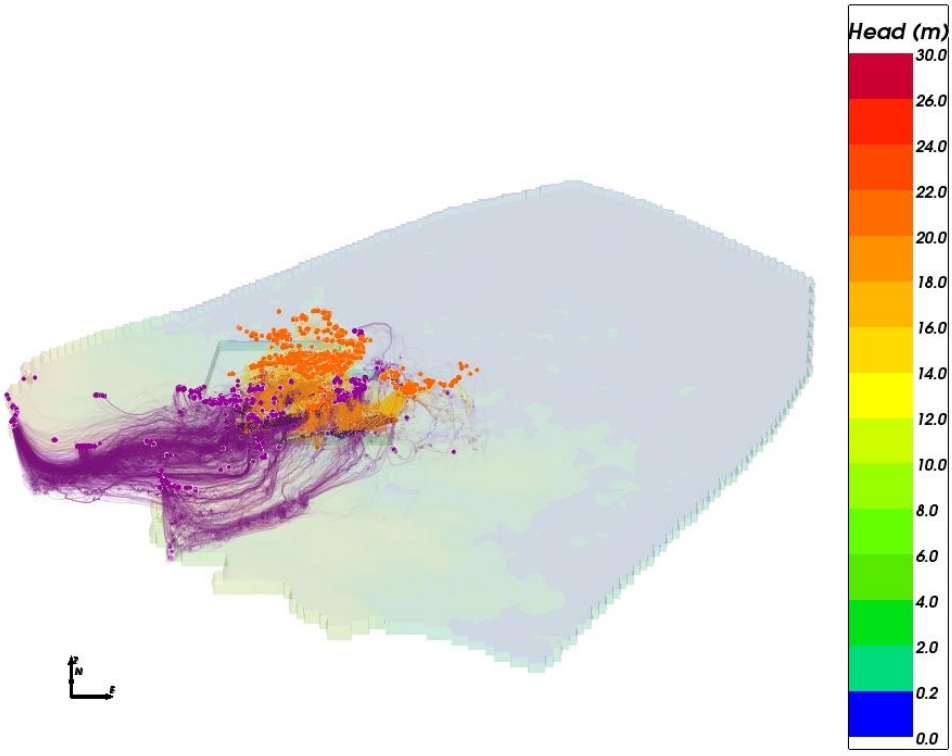

Figure 2-14. *Simulations of discharge pathways (orange) and recharge pathways (purple) for a release from all deposition holes in the flow field under temperate conditions at 2000 AD. [Part of Figure F-2 from Joyce et al. (2010a)]. Many pathlines are truncated at the boundary of the domain which suggests predicted dilution times could be (cautiously) underestimated to some extent.*

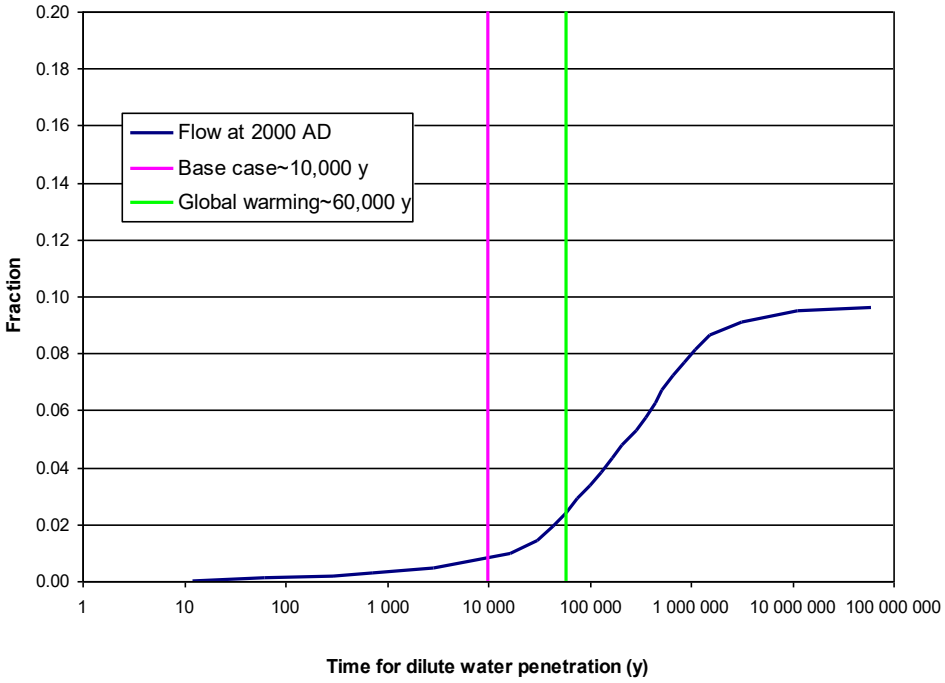

Figure 2-15. *Estimates of time for penetration of dilute groundwater under temperate conditions expressed as fraction of deposition holes experiencing dilute conditions. The vertical lines indicate the duration of the initial temperate period: Base case ~10,000 years (purple), Global warming variant~60,000 years (green). (Figure F-8 from Joyce et al. 2010a). Note that of the 6916 deposition holes, only 663 or around 10% were found to have complete flow paths to the surface (hence the asymptote at that fraction in the plot).*

2.2 More recent work

2.2.1 Longer-term hydrogeochemical evolution at Forsmark

Following SR-Site, an additional capability to couple groundwater flow and transport with chemical reactions was added to ConnectFlow (Joyce et al. 2014a) for CPM and ECPM models. This was implemented by linking ConnectFlow to the iPhreeqc library (Charlton and Parkhurst 2011), which provides access to the full range of chemical modelling facilities in PHREEQC (Parkhurst and Appelo 1999). Specified chemistry calculations can be carried out at the end of each time step of a groundwater flow and transport calculation to adjust the geochemical composition at each location in the model, including within the rock matrix. Geochemical calculations were facilitated in the rock matrix by providing an alternative implementation of rock matrix diffusion whereby the rock matrix is discretised using a finite volume representation. This representation allowed geochemistry to be calculated in individual cells within a 1D discretisation of the rock matrix for each ECPM cell in the ConnectFlow model. Including geochemical reactions necessitated simulating the transport of individual chemical components, rather than reference waters, because the chemical reactions meant that groundwater composition could no longer be expressed solely as the mixing of different proportions of reference waters. Due to the increased computational burden of the additional capabilities, parallelisation of the code was introduced to improve efficiency. Repository structures were not included in the models, an approximation which therefore ignores the impact these structures could have on inflow paths.

The additional ConnectFlow functionality to carry out groundwater flow, solute transport and geochemical calculations was applied to the regional-scale model from SR-Site but for an extended temperate climate period of up to 60,000 AD (Joyce, et al. 2014b). This extended period could be a result of climate warming and has the potential to expose the site to a longer period of meteoric water infiltration. The longer period of infiltration could in turn lead to increased dilution of the groundwater at repository depth. However, the simulations showed that the penetration of dilute groundwater to repository depth was relatively limited, and didn't increase appreciably after about 20,000 AD. This limited dilution was a consequence of the low permeability of the bedrock which led to groundwater flow being predominantly in the shallow bedrock aquifer. By contrast,

groundwater flow at depth was slow and limited by the low permeability of the fractured bedrock. Rock matrix diffusion also played a role in reducing the rate of penetration of dilute groundwater to repository depth. Geochemical reactions had little effect on total salinity, as salinity is dominated by dissolved sodium chloride, which is relatively unaffected by the chemistry (see, for example, Figure 2-16 and **Fel! Hittar inte referenskälla.**). However, there was a minor effect on the concentrations of some reactive species for the chemical reactions considered, but not to the extent that the SR-Site safety functions would be affected.

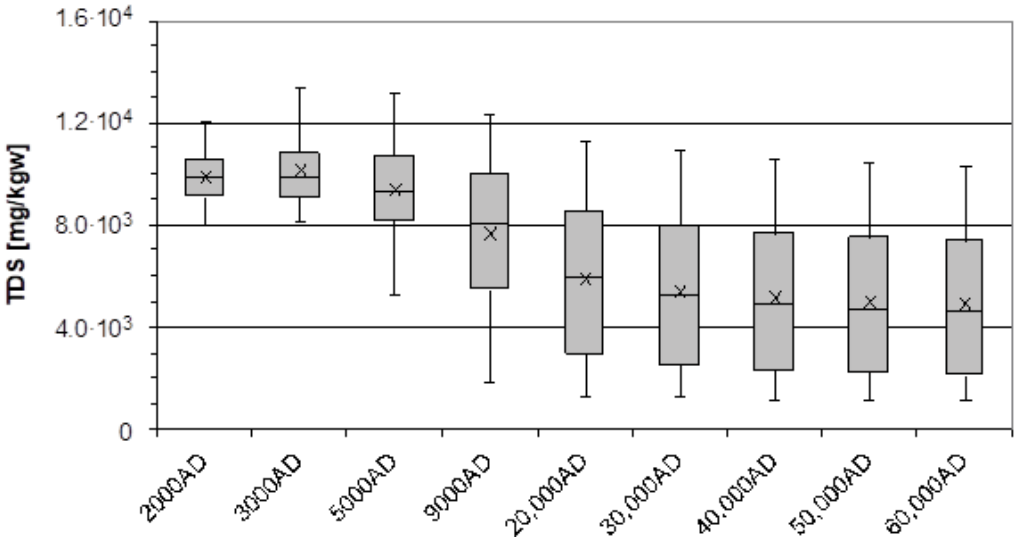

Figure 2-16. *Box and whisker plot showing the statistical distribution of Total Dissolved Solids (TDS) on a regular grid of points within the repository volume between elevations -490 m and -460 m. The statistical measures are the median, the 25th and 75th percentiles (box), the mean (cross) and the 5th and 95th percentiles (whiskers). [Figure 4-35 in Joyce et al. (2014b)].*

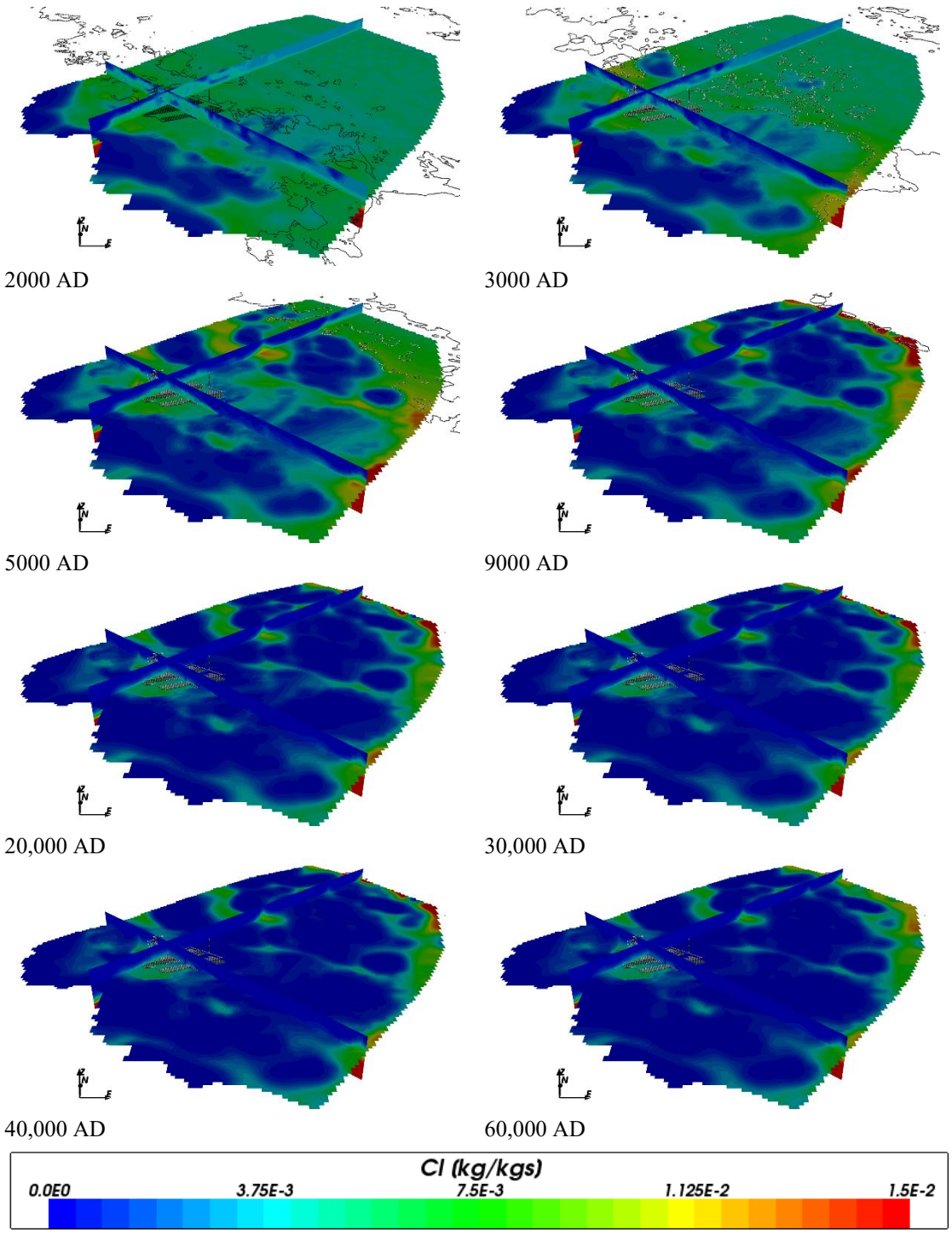

Figure 2-17. *Total chloride mass fractions on regional scale slices through the repository volume for time periods 2000 AD to 60,000 AD [Figure 4-48 in Joyce et al. (2014b)]. The repository structures and the time-varying coastline are shown in black (repository structures are for reference only, they are not included in the model).*

2.2.2 Further calculations of dilute water penetration at Forsmark

As part of the work for the Preliminary Safety Assessment Report (PSAR) for a spent nuclear fuel repository at Forsmark (SKB 2022a), the particle-based analytical approach to calculating dilution of groundwater was developed further (SKB 2022b). This approach considered that some of the simplifying assumptions used in the SR-Site approach (Joyce et al. 2020a) summarised in Section 2.1.6 were too cautious. In particular, the assumptions: that the rock matrix is infinite; that infiltrating water has zero salinity; and that the flow paths interact only with the surrounding rock matrix. For PSAR, a new particle-based method for calculating dilution was developed whereby groundwater flow in fractures was restricted to channels with adjacent stagnant zones. Both the flow channels and the stagnant zones were considered to be in contact with the rock matrix. Therefore, solute transport could be through the flow channels (advection), between the flow channels and the stagnant zones (diffusion) or the rock matrix (matrix diffusion), and also between the stagnant zones and the rock matrix (matrix diffusion). The rock matrix was represented as having a finite extent.

The method developed for PSAR was based on work described in Mahmoudzadeh et al. (2013), but for a specified constant inlet salinity and for a single constant initial salinity throughout the fractures (flow channels and stagnant zones) and rock matrix. The method uses a Laplace transform approach, with the equations solved in the four subsystems (flow channels; stagnant zones; rock matrix adjacent to flow channels; rock matrix adjacent to stagnant zones), with the assumption of continuity in salinity between each of the subsystems. The approach yielded the following equation:

$$\bar{C}_f(x,s) = \frac{C_0}{s} + \frac{C_{in}-C_0}{s} exp\left(-\Omega_f - N\sqrt{\Omega_s}\tanh\left(2\sqrt{\Omega_s}\right)\right) \quad (2.2)$$

where $\bar{C}_f$ is the salinity in the flow channel (the overbar indicating a Laplace transformed quantity), x is the distance along the flow direction, s is the Laplace transform variable, N accounts for the fraction of solute that can depart from the flowing channel into the stagnant water zone, while Ω_f and Ω_s describe the interaction of the rock matrix with the flowing channel and stagnant zones, respectively [see SKB (2022b) for details].

The new method was applied to conditions corresponding to those used in SR-Site for different climate states. When parameterised in a way that was equivalent to the SR-Site method (e.g. zero stagnant zone width), very similar results were obtained (e.g. Figure 2-18). However, in general, the new method showed reduced dilution of deposition hole locations (e.g. Figure 2-19, corresponding to the case propagated for PSAR). Note that the threshold salinity for onset of erosion is set to 0.6 g/L for PSAR compared to 0.3 g/L for SR-Site.

Separately, in Appendix J of SKB (2022b), scoping geochemical calculations based on updated SR-Site models indicate that the rate of calcite depletion from recharge flow paths is slow, even during dilute glacial infiltration periods. Furthermore, matrix weathering of oligoclase appears capable of sustaining or replenishing Ca^{2+} in fracture water, particularly if effective diffusivity in the alteration zone remains high. This result suggests that Ca^{2+} capacity persists for long durations and may contribute to sustaining salinity levels above critical thresholds, even in long-term temperate or glacial periods.

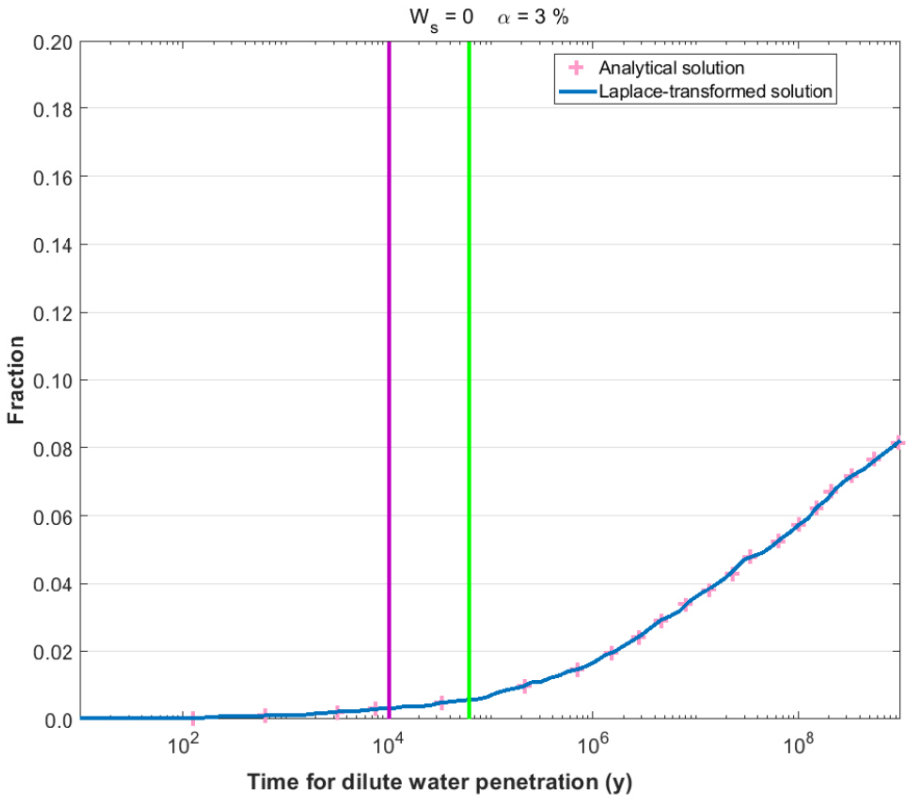

Figure 2-18. *Estimates of time for penetration of dilute groundwater under temperate conditions with no stagnant water zone, a dilution factor (α) of 3%, zero inlet salinity and infinite rock matrix (Laplace-transformed solution), compared to SR-Site (analytical solution). The vertical lines indicate the duration of the initial temperate period: Base case~10,000 years (purple), Global warming variant~60,000 years (green). [From Figure K-9 in SKB (2022b)].*

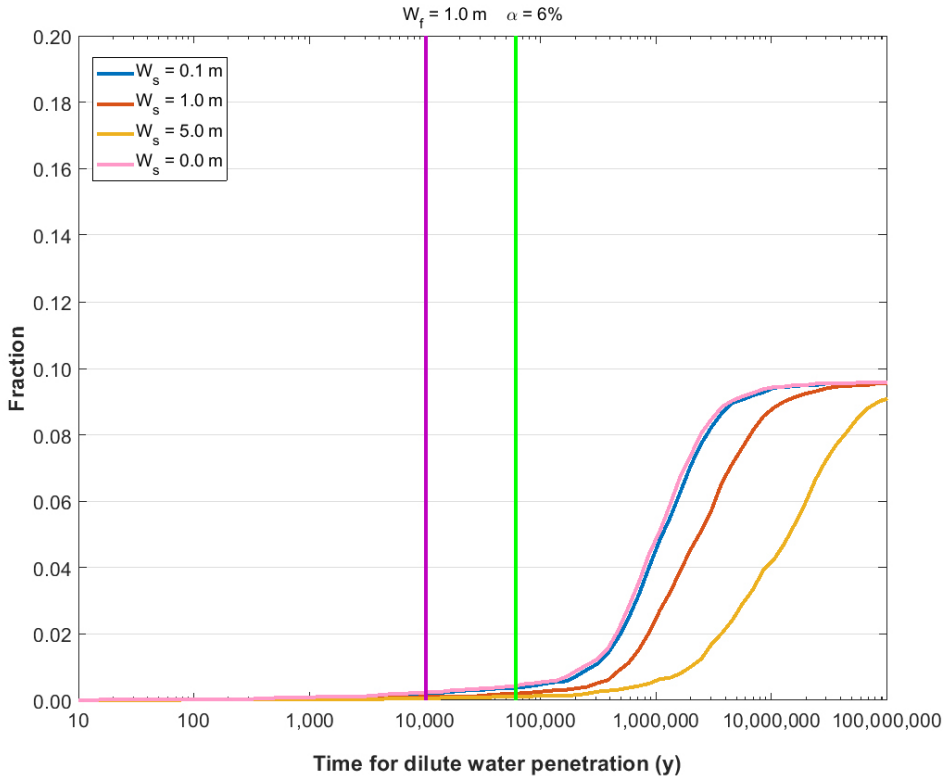

Figure 2-19. *Estimates of time for penetration of dilute groundwater under temperate conditions for a flow channel half-width (wf) of 1.0 m, a dilution factor (α) of 6%, an inlet salinity of 0.4 g/L and various half-distances between flow channels (ws). The vertical lines indicate the duration of the initial temperate period: Base case~10,000 years (purple), Global warming variant~60,000 years (green). [From Figure K-6 in SKB (2022b)].*

2.2.3 Dilution of groundwater at Olkiluoto

As part of the support to the Posiva Safety Case for the Operating License Application (SC-OLA) for a spent nuclear fuel repository at Olkiluoto in Finland, Hydrogeological and Hydrogeochemical Evolution Modelling (HHEM) calculations were carried out (Joyce et al. 2021). The approach was very similar to that used for SKB's SR-Site, with an ECPM representation of the bedrock upscaled from an underlying DFN model of the fractured crystalline rock. However, each deterministic feature, i.e. each Brittle Fault Zone (BFZ), was conceptualised as a swarm of enhanced fracturing within a planar volume. Although chemical reactions were not included, the simulations were carried out using a similar approach to that outlined in Section 2.2.1, i.e. by calculating the transport of individual chemical species. Depending on the climate case, simulations were run over timescales of up to 120,000 years, representing either a single temperate period or a complete temperate– glacial cycle. These simulations allowed for the estimation of groundwater composition changes over time (e.g., see Figure 2-20).

The grid scale (30 m) used for the HHEM simulations was too coarse to calculate dilution at individual deposition hole locations. Therefore, a particle-based approach was adopted (Posiva 2021), similar to those described in Sections 2.1.6 and 2.2.2. Backward particle tracks were calculated in DFN models of the Olkiluoto bedrock using steady-state conditions exported from the ECPM models at specific time points. These backward particle tracks represented routes for the penetration of meteoric or glacial water with the potential to dilute deposition hole locations to below the SC-OLA criteria used to indicate the onset of chemical erosion, expressed as a total cation concentration of either 8 meq/L ("reference" criterion) or 12 meq/L (more cautious "alternative" criterion).

Posiva (2021), Appendix C, describes how the solute concentrations at a deposition hole were determined using data from 1D advective pathlines. The properties of the rock matrix are defined by the DFN elevation region and whether it is adjacent to a BFZ or a background fracture. The rock matrix porewater composition is based on a layered structure of water types:

- Fresh/brackish HCO3 type water at shallow depth from overburden down to a depth of 100 m;
- Brackish SO4 type water from 100 m depth to a depth of 300 m;
- Brackish/saline Cl type water below 300 m.

A semi-analytical approach is used to include the effect of matrix diffusion on the dilution process. The flow path is split into segments, each with uniform initial salinity and matrix properties. For each segment of the flow path, the response function for retention is calculated using the approach given in Poteri (2009); this function characterises the time-dependent relationship between the input and output solute concentrations, accounting for advection in the fracture and retention by matrix diffusion within the segment. The method assumes linear transport, allowing the response function to be applied through convolution with the input concentration signal (Posiva 2021, Appendix C):

$$C_f(t) = C_0 + \int_0^t (f(\tau) - C_0) g(t-\tau) d\tau \quad (2.3)$$

where Cf(t) is the fracture outlet concentration at time t, C0 is the initial concentration in the rock matrix, f(τ) is the concentration flowing into a fracture and g(t – τ) is the response function, as discussed in (Posiva 2021, Appendix C).

The overall solution is obtained by sequentially applying the response functions along the flow path. The output from one segment becomes the input to the next, allowing the cumulative effect of multiple retention processes in series to be represented. This approach allows for variation in flow and matrix properties between segments and does not require solving the coupled transport equations over the entire domain. Longitudinal dispersion and diffusion within the fractures are neglected.

When compared to the equivalent PSAR approach (SKB 2022b), the approach taken by Posiva (Posiva 2021, Appendix C) relaxes the assumption of uniform initial solute concentrations and uniform matrix properties while ignoring diffusion into the stagnant areas of fractures and the matrix adjacent to those stagnant areas.

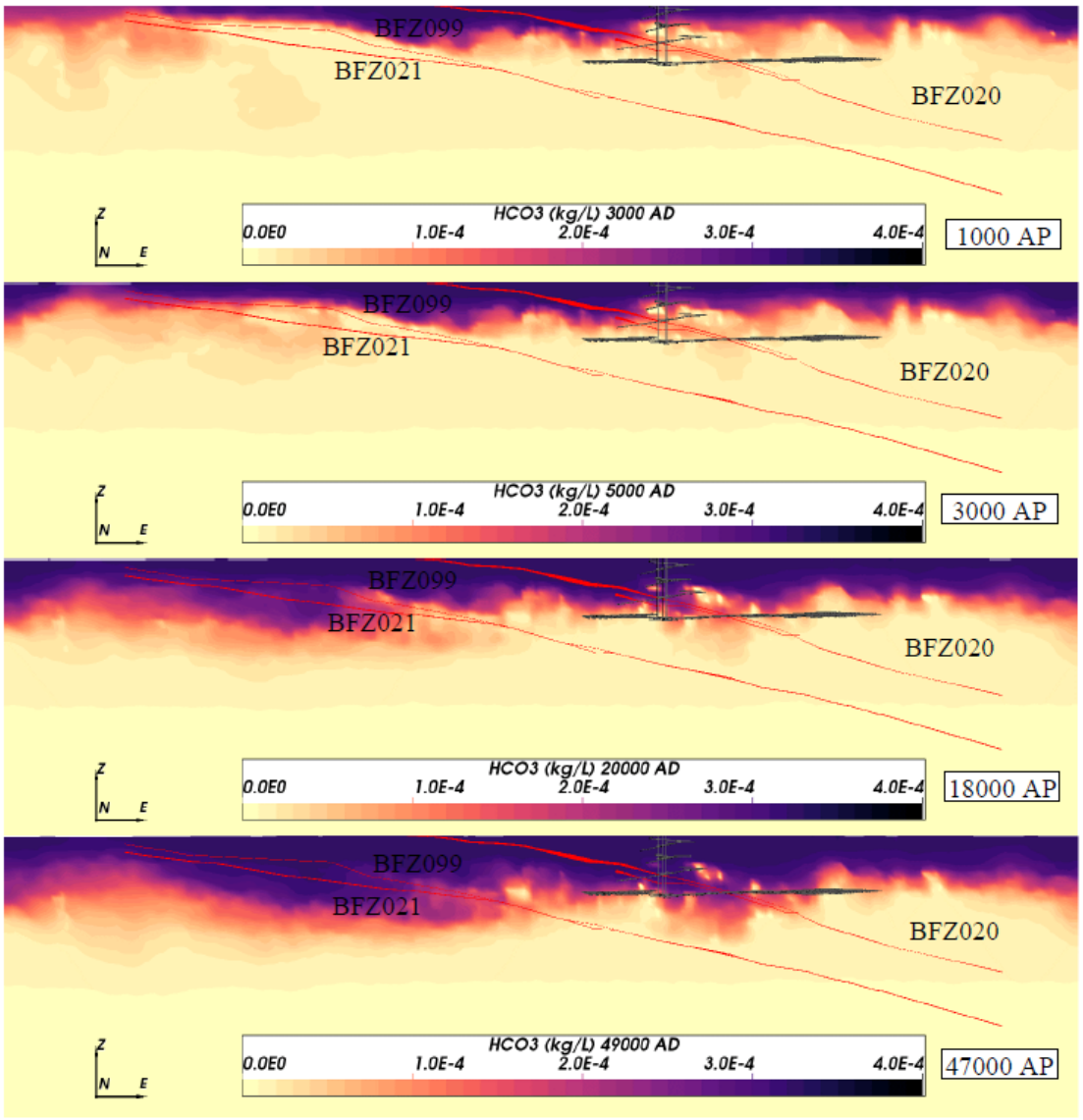

Figure 2-20. *Bicarbonate concentration in fracture groundwater at different times during the initial post-closure temperate period for the global warming climate line of evolution on a vertical west-east slice through realisation 1 of the SC-OLA HHEM model. Major BFZs are shown in red for context and the repository openings are shown in black. [Figure 4-9 in Joyce et al.(2021)].*

Calculations of dilution times were carried out for backward particle tracks released from each deposition hole intersected by a fracture, where the particle successfully reached the ground surface. In some cases, particles were excluded if they did not meet Posiva's Rock Suitability Criteria (RSC). Only particle segments within the bedrock or tunnels were considered, i.e. overburden segments were excluded. One particle was released from each deposition hole location for 10 realisations of the DFN to assess variability between realisations. For one realisation, 10 particles were released from each deposition hole location to assess variability between flow paths. Example results are shown in Figure 2-21, which indicate that variability between realisations is a little greater than variability between flow paths. When compared with PSAR, these Posiva calculations predict that a larger number of deposition holes will experience dilution. This is most likely due to the higher fracture intensity (of flowing fractures) in the Olkiluoto bedrock, resulting in larger numbers of fractures intersecting with boreholes and larger flow rates.

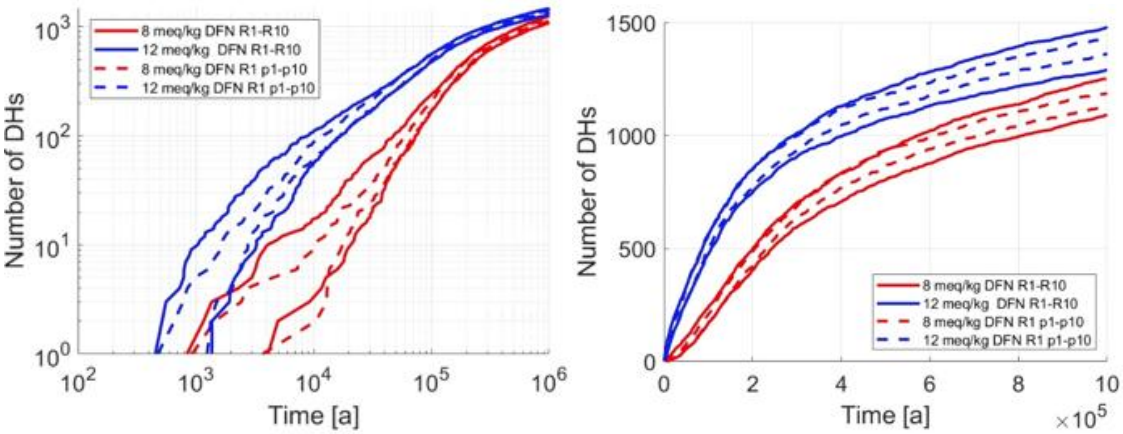

Figure 2-21. *Variability in dilution time distributions (the number of deposition holes (DHs) showing dilution, where the total number of DHs was 3978) over ten recharge paths per deposition hole (dotted lines) or one recharge path per deposition hole over ten DFN realisations (solid lines) on a log-log scale (left) or a linear scale (right). Only the bounding distributions of the swarm of curves are shown.[Figure 17 in Posiva (2021)].*

The ECPM approach was found to be insufficiently tractable to be used for dilution calculations over the entire simulation period (400,000 years which covered the temperate period of an Extended Global Warming variant). Instead, the more tractable pathline method was used to predict the dilution for the simulation period. Additionally, a comparison was made between the dilution predictions of pathline based methods, and ECPM methods, over a shorter period (120,000 years). This comparison showed reasonable agreement when performed for an average of all deposition holes in the entire repository. It was noted that the ECPM models had greater mixing/dispersion than the pathline methods, because mixing was available along the whole flow path rather than just at the deposition hole. It was also noted that the ECPM cell size of 30 m will tend to cause surplus mixing; for example, a distance of 30 m will cover several deposition hole locations simultaneously.

This work highlights several aspects of ECPM and pathline based methods. ECPM methods may result in surplus mixing/dispersion and can be computationally intractable. Pathline based methods are more tractable but still have difficulty representing mixing and dispersion adequately.

3 Modelling solute transport using DFNs

Section 2 described previous work considering dilute water penetration which has typically relied on an ECPM approach or used pathline-based models to represent solute transport within fractured host rock. Both methods make significant approximations, with the former averaging the hydraulic properties of fractures within potentially quite large volumes of rock and the latter approximating dispersion and ignoring the initial complex distribution of solutes within the fractures and matrix. A more natural approach is to use DFN representations of the host rock to directly calculate the flow and transport within and between fractures. Each fracture is discretised using a two-dimensional mesh; then the flow, transport and reaction equations are solved on an intersecting network of these two-dimensional meshes.

3.1 DFN flow and transport equations

The equations below represent Darcy flow, and the transport of n solutes $c_i = c_1, c_2, \ldots, c_n$ through a single fracture. The diffusion of solutes into the surrounding rock matrix is explicitly included, but unsaturated groundwater flow and heat transport are not considered.

$$\frac{\partial}{\partial t}[e_t \rho(c_i, P_R)\,] + \vec{\nabla} \cdot \left[\rho(c_i, P_R)\vec{Q}\right] = 0 \tag{3.1}$$

$$\frac{\partial}{\partial t}[e_t \rho(c_i, P_R) c_i] + \vec{\nabla} \cdot \left[\rho(c_i, P_R)\vec{Q} c_i\right] = \vec{\nabla} \cdot \left[e_t \rho(c_i, P_R) D \cdot \vec{\nabla} c_i\right] + 2\rho(c_i, P_R) D_i \left.\frac{\partial c_i'}{\partial w}\right|_{w=0} \tag{3.2}$$

$$\vec{Q} = \frac{e_h^3}{12\mu(c_i, P_R)}\left[\vec{\nabla} P_R - (\rho(c_i, P_R) - \rho_0) g \vec{z}\right] \tag{3.3}$$

$$\alpha \frac{\partial}{\partial t}[\rho(c_i, P_R) c_i'] = \frac{\partial}{\partial w}\left[D_i \rho(c_i, P_R) \frac{\partial \rho(c_i', P_R) c_i'}{\partial w}\right] \tag{3.4}$$

Here, n versions of Equations (3.1) to (3.4) are required to model the transport of n solutes. Equation (3.4) is usually simplified by assuming constant density within the matrix. The variables referred to are:

- P_R [Pa] the residual pressure: $P_R = P_T + \rho_0 g z$; (where g is the acceleration due to gravity, z is the elevation above sea level, P_T is the total pressure and ρ_0 is a reference density);
- c_i [-] the mass fraction of solutes in the fracture;
- c_i' [-] the mass fraction of solutes in the matrix;
- e_h [m] the effective hydraulic aperture in the fracture;
- e_t [m] the transport aperture in the fracture;
- $\rho(c_i, P_R)$ [kg m^{-3}] and $\mu(c_i, P_R)$ [kg m^{-1} s^{-1}] the fluid density and viscosity, respectively. Density and viscosity can be calculated using empirical expressions [16];
- $\vec{Q}$ [m^2 s^{-1}] the volume of water flowing per second, per unit width of the fracture;
- t [s] the time;
- $\vec{\nabla}$ the two-dimensional gradient operator within the fracture;
- D [m^2 s^{-1}] the dispersion tensor within the mobile water in the fracture; the dispersion tensor includes contributions from diffusion and from hydrodynamic dispersion; the latter has components parallel and perpendicular to the flow;
- D_i [m^2 s^{-1}] the intrinsic diffusion coefficient for diffusion into the rock matrix;
- w [m] the perpendicular distance from the fracture plane into the rock matrix;
- α [-] the capacity factor (when there is no sorption, the capacity factor is the same as the porosity of the matrix).

These equations are analogous to those used in ConnectFlow for a continuous porous medium (CPM) (Joyce et al. 2014), and have been implemented within ConnectFlow's DFN module. The viscosity and density are dependent on the solute concentrations, and hence couple together the groundwater flow and transport equations (the equations can be simplified by removing this dependency).

Equations (3.1) to (3.4) do not include chemical reactions. Chemical reactions, involving solutes and rock minerals, within the fracture porewater and the rock matrix, have also been implemented for DFNs in ConnectFlow. However, this capability is not used in the current work.

3.2 Numerical approach and discretisation

The DFN module of ConnectFlow uses a Galerkin finite-element approach and two levels of discretisation: a fine-scale discretisation on individual fractures, and a coarser scale for the whole network. For the whole network, pressure and solute concentrations are defined at "global nodes" which exist on the intersections between fractures. Following the Galerkin approach, each global node on a fracture has an associated basis function. The form of these basis functions is key to the ConnectFlow algorithm. They are calculated by solving the groundwater flow equations (using the fine-scale discretisation) on each fracture in isolation using a particular set of boundary conditions for each basis function/global node (specifically a delta function with value 1 at the global node in question and 0 for the other global nodes). Once the basis functions are defined, the global system of equations can then be assembled and solved.

Thus, groundwater flow calculations proceed in two stages (Figure 3-1); first the global basis functions are calculated within each fracture; next, the equations for the flow in the overall network are assembled and solved.

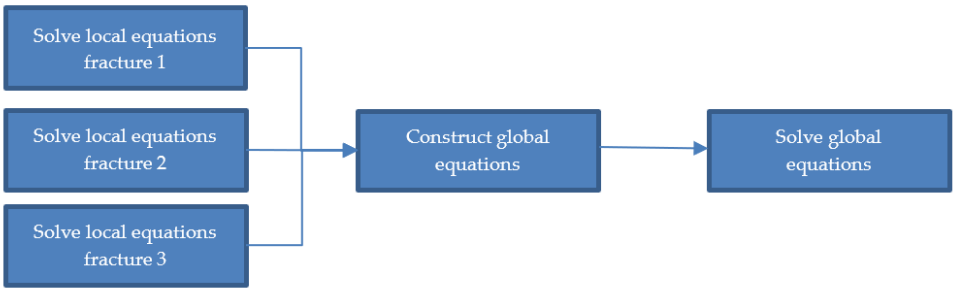

Figure 3-1: *In ConnectFlow, DFN simulations are performed in two steps. Firstly, a series of calculations are done for each individual fracture (each calculation determines a global basis function). The global basis functions are then used to build the global equations which are then solved. [Figure 1 from Applegate and Appleyard (2022)].*

A similar process is followed when calculating solute transport. Note, the global basis functions are not appropriate for representing large variations of salinity within a single fracture. If large variations are expected, then the fractures should be tessellated into smaller sub-fractures. The fracture tessellation length should be smaller than the longitudinal dispersion length.

While this approach is very efficient, solute transport calculations are nevertheless challenging. Parallelisation is therefore used to further enhance the performance. In particular, the calculation of the basis functions (Figure 3-1) is readily split across multiple processors.

3.3 Rock matrix diffusion

A numerical scheme for determining the diffusive flux between the mobile porewater and the matrix, for an upscaled ECPM model, is presented in Joyce et al. (2014). A similar approach is used in ConnectFlow to represent the rock matrix in a DFN (see Figure 3-2). Using a one-dimensional finite volume discretisation, and assuming the fluid density in the matrix is constant, Equation (3.4) becomes

$$\frac{\alpha\left(c'^{n}_{j}-c'^{n-1}_{j}\right)}{\Delta t}=\frac{2D_j}{\Delta w_j}\left\{\frac{\left(c'^{n}_{j+1}-c'^{n}_{j}\right)}{\Delta w_j+\Delta w_{j+1}}-\frac{\left(c'^{n}_{j}-c'^{n}_{j-1}\right)}{\Delta w_{j-1}+\Delta w_j}\right\}. \tag{3.5}$$

The term in Equation (3.2) representing the diffusive flux F (advection into the matrix is ignored) between the fracture and the surrounding matrix becomes

$$F = \frac{4\rho D_i}{\Delta w_1}\left(c'^{n}_{1} - c^{n}_{j}\right) \tag{3.6}$$

where the index j indicates the finite volume (note we have dropped the species index here), with index $j = 1$ representing the volume adjacent to the fracture; and index n indicates the time step. Following the derivation from Joyce et al. (2014), Equation (3.5) can be written in the following form:

$$F = A^n + B\frac{c^n - c^{n-1}}{t^n - t^{n-1}} \tag{3.7}$$

where c^n is the solute concentration in the fracture system at the end of time step n, and the coefficients A^n and B do not depend on c^n. Conveniently, A^n and B are calculated from matrix concentrations at previous time steps. This fact means that the calculation of the fracture and matrix concentrations can be carried out sequentially, significantly reducing the computational burden.

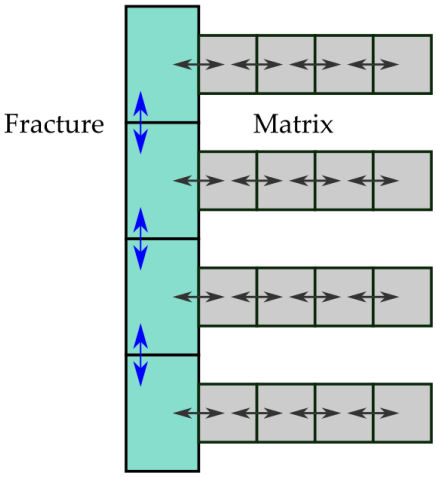

Figure 3-2: *Schematic of transport within the fracture and the matrix. The blue arrows indicate advective-diffusive transport between sub-fractures; the black arrows indicate diffusive transport between the fracture and the matrix, and also within the matrix. [Figure 3 from Applegate and Appleyard (2022)].*

Fractures are typically tessellated into smaller sub-fractures with diffusion between fractures and the matrix calculated at the centre of each sub-fracture. The number of sub-fractures within a fracture can be increased to improve the accuracy of the calculation.

Rock matrix diffusion calculations are defined according to the following parameters:

- The total diffusion length into the matrix $w_{max} = \sum_{j=1,n_{fv}} w_i\ [m]$;
- The number of finite volume cells per global node, n_{fv};
- The intrinsic diffusion coefficient, D_i [m^2/s];
- The porosity of the matrix or capacity factor, α [-].

The total diffusion length into the matrix can either be directly specified or calculated from the average distance to the adjacent fractures, noting that diffusion of solutes can propagate through a matrix block from fractures on both sides. For non-parallel fractures, the shortest distance between the fractures varies over the fracture surface. Fracture tessellation is once again beneficial since each sub-fracture has its own diffusion length allowing this quantity to vary over a tessellated fracture. Note that in this report (see Section 4.4) the matrix diffusion length has been specified by rock type rather than automatically calculated.

3.4 Reference waters

Reference waters are solutions with defined, fixed, solute compositions. Reference waters are useful when there are mixtures of groundwaters with identifiable origins, for example glacial meltwater, meteoric water or sea water, and when there are more dissolved solute species of interest m than reference waters n. In a transport calculation it is then more efficient to solve for the transport of the reference waters than the individual solutes.

Consider a mixture of n reference waters, each with a specified composition of m solutes. The sum of the reference water fractions F_w must equal one ($\sum_{w=1,n} F_w = 1$). ConnectFlow solves the transport equation for each reference water (the fraction of the last reference water is inferred trivially from the others). The mass fraction of a solute species i, can then be obtained from the fraction of each reference water F_w and the mass fraction of species i contained within that reference water $c_{i,w}$.

$$c_i = \sum_{w=1,n} F_w c_{i,w} = \sum_{w=1,n} \left(\frac{F_w M_{i,w}}{M_{wat} + \sum_{j=1,m} M_{j,w}} \right) \tag{3.8}$$

where the mass fraction, c, of a solute species, i, is defined by the mass of this species, M_i, the mass of water, M_{wat}, and the mass of all solute species, M_j.

4 Model description

4.1 Model Domain

The simulation domain specified for this work is the repository-scale block 1, defined for SR-Site. This domain has dimensions of 2095 m x 1267 m x 800 m and covers a vertical extent from -800 m elevation to the ground surface (the deposition tunnels are located at roughly -470 m depth). The block 1 domain covers approximately a third of the disposal area and a small proportion of the regional model described in SR-Site (See Figure 4-1).

The near-surface geology of the Forsmark site has up to several metres of quaternary deposits. It is not possible to represent these deposits using a discrete fracture network (DFN) on its own. Therefore, these deposits have not been included in the DFN calculations (or the ECPM calculations for consistency). Ideally, a combined CPM-DFN model would be used to represent the site, but this functionality was not available within ConnectFlow (for advection-diffusion calculations) at the time these calculations were carried out. Surface boundary conditions are therefore applied directly to the top of the fractured rock rather than the top of the quaternary deposits.

The calculations presented in this report do not include the repository structures for simplicity. These repository structures are sometimes shown in figures for reference purposes. While it is noted that the tunnels could affect flows in their vicinity, the motivation of this work is to compare different simulation methods, and it is therefore reasonable to simplify the model in this regard.

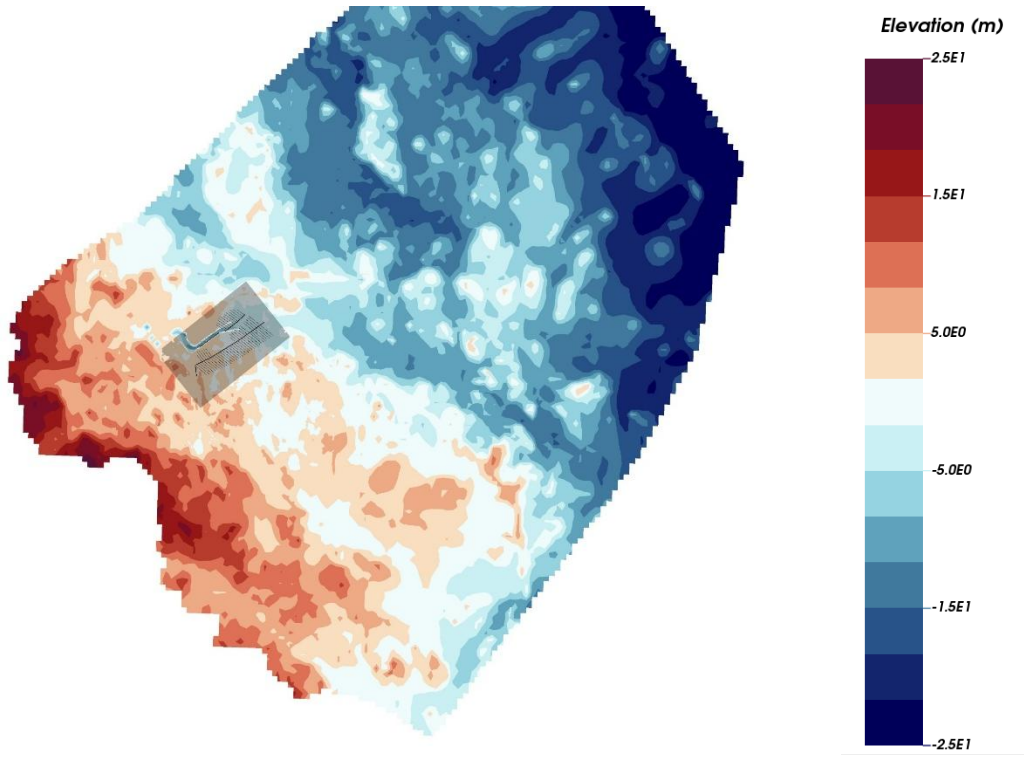

Figure 4-1: *The SR-Site regional scale model coloured by surface elevation. The extent of the repository block 1 model is shaded grey.*

4.2 Fracture System

Twenty-four deformation zones (DZs) are known to pass through the model region. Physically, these deformation zones are composed of clusters of much smaller fractures. In SR-Site (Joyce et al. 2010a) the DZs were represented using planar DZ features, rather than representing the smaller constituent fractures. More recent advances (Hartley et al. 2018) have suggested that the DZs could be better represented using swarms of stochastically generated fractures.

In the current report the fractures are represented using a plane-projection technique which takes the swarm fracture representation and then projects the hydraulic properties onto planar features. This approach can provide similar advective transport properties compared to the fracture swarm method (Williams et al. 2021) but is also more efficient numerically. Figure 4-2 and Figure 4-3 show the original swarm and plane-projected DZ features.

In addition to DZs, random background fractures and sheet-join fractures have been included in the model. The random background fractures included are those generated for SR-site, while the sheet joins have been represented as planar features (Figure 4-4), rather than fracture swarms.

The minimum fracture size included in the model is 5 m in length. This cut-off length is larger than that used in SR-Site (Joyce et al. 2010a) where the minimum fracture size ranges from 0.7 m to 10 m depending on the distance from the repository structures. The reason for using a larger cut-off is to reduce the number of fractures, which in turn improves tractability of the DFN transport calculations. The impact of small fractures on transport through a fracture network is likely to be small since the aperture and corresponding flow rate through these fractures will be small. (This will limit advective transport, while diffusive transport is typically of lower importance, especially when compared with overall transport in larger aperture fractures).

Large fractures are tessellated into smaller sub-fractures, 20 m in length. This tessellation length determines the smallest length scale of concentration variation that can reasonably be represented within ConnectFlow. Thus, the longitudinal dispersion length must be greater than or equal to the tessellation length. (The situation with pressure solves is slightly different; pressure variations that are smaller than the tessellation length, but larger than the finite element size, can be modelled successfully).

Fracture removal is important for the numerical stability of DFN calculations. The following fractures have been removed from the model because they are likely to be non-percolating or may cause numerical issues:

- Fractures/clusters of fractures that are isolated (have no connection to the model boundary either directly or via connections with other fractures).
- Fractures/clusters that are pinched (only connect to the rest of the fracture network or a boundary via a single fracture intersection).

It is acknowledged that these non-percolating fractures could play a role in the transport of solutes via diffusion. However, their surface area (for fracture lengths greater than 5 m) is small (about 10%) compared to the rest of the network. It is also possible for the impact of non-percolating fractures to be approximated using additional rock matrix diffusion, if required.

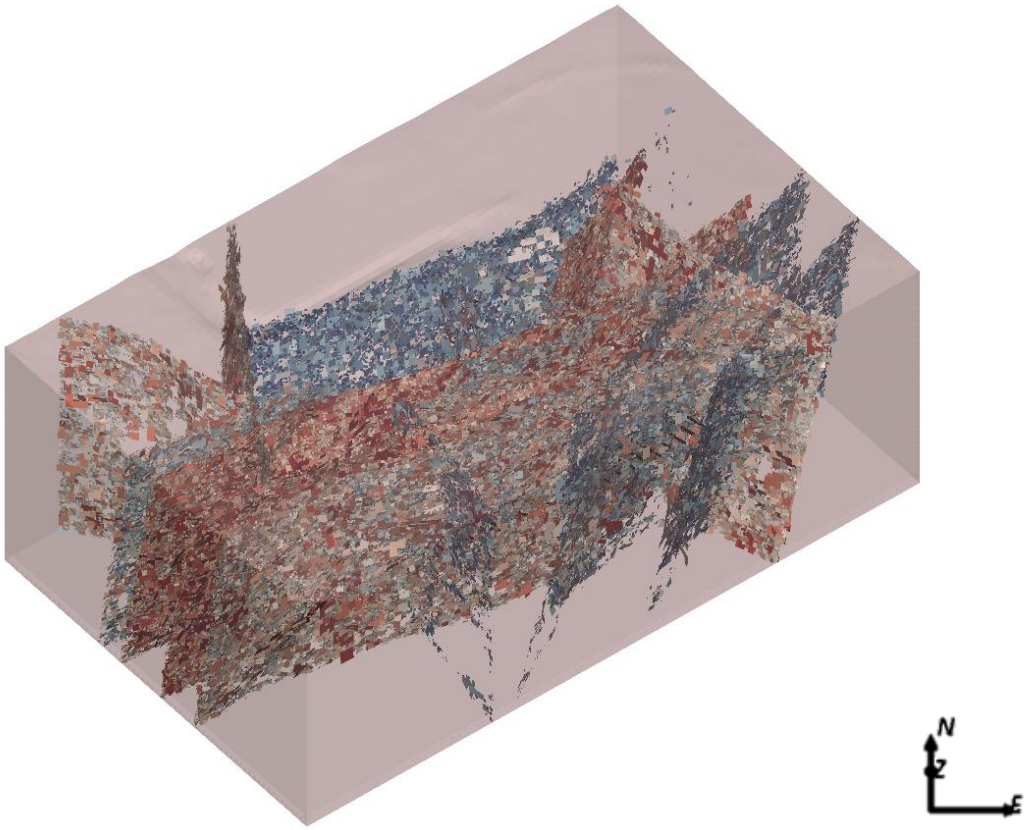

Figure 4-2: *Deformation Zones represented as fracture swarms.*

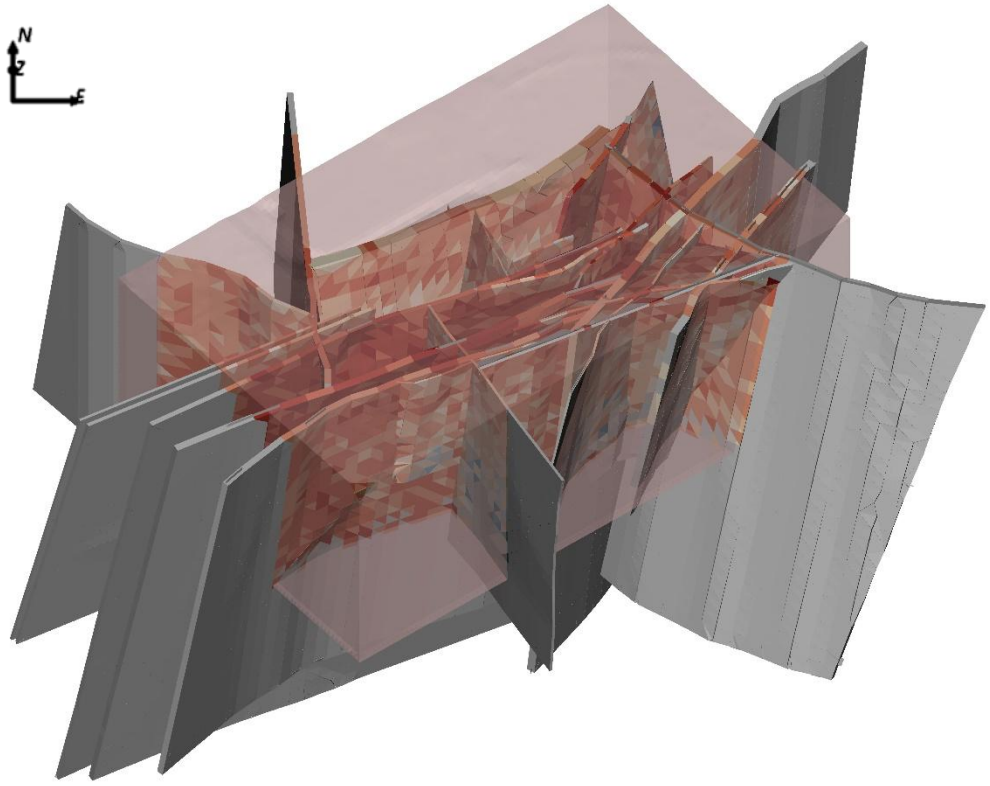

Figure 4-3: *Deformation Zones represented using the plane-projection method.*

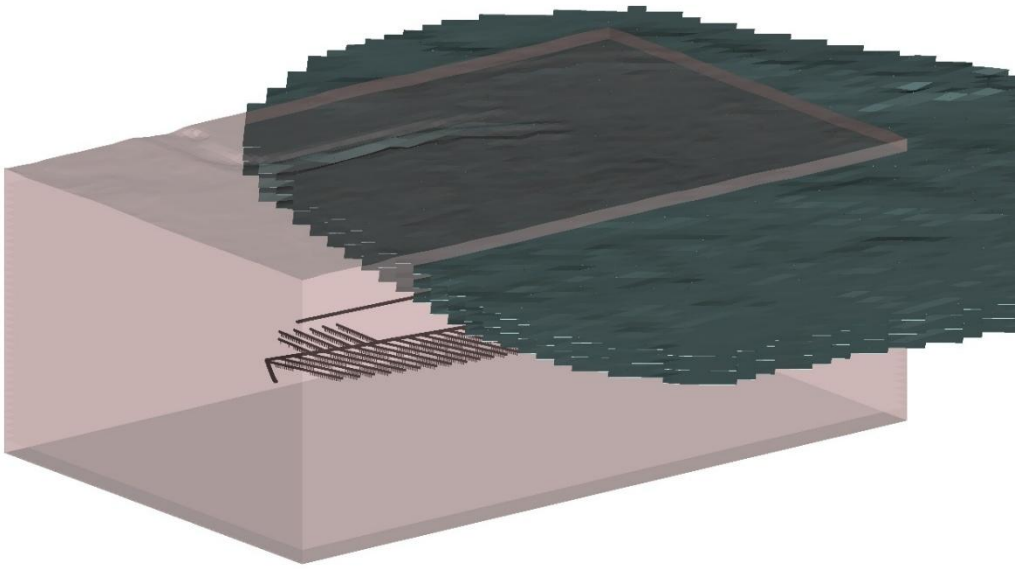

Figure 4-4: *Sheet join fractures, each represented as a single plane.*

4.3 Groundwater composition

The regional transport calculations in SR-Site (Joyce et al. 2010a) define five reference waters. These reference waters define key water compositions that have been present at the Forsmark site in the last 10,000 years. Table 2-1shown previously, lists the properties of these five reference waters.

In the original SR-Site regional model these five reference waters were transported simultaneously within an ECPM representation of the fracture system. Explicit DFN simulations with large numbers of solute species have been demonstrated for for SFL (Applegate and Appleyard 2022). In the latter case, however, it was noted that those calculations required significant computational resources, even with the efficient algorithms used in ConnectFlow. This has motivated the development of a simplified approach, where the total salinity is transported rather than five separate species. This has been done by using two reference waters, one fresh and one saline (see Table 4-1). Five reference water calculations were also carried out using modified boundary conditions to improve their tractability.

Table 4-1: Two reference waters can be used to represent the transport of basic salinity. The properties of these two reference waters are given below for the Forsmark site.

	Density [kg·m−3]	Total dissolved solids [kg·m−3]	Salinity [-]	Viscosity [kg·m−1·s−1]
Fresh water	998.22	0.00200	2.00×10^{-6}	1.00×10^{-3}
Saline water	1049.8	75.1	7.15×10^{-2}	1.12×10^{-3}

Although two reference waters cannot fully replace the information provided by five reference water calculations, modelling the evolution of the total salinity is still a useful indicator for the purpose of buffer and canister performance. Note that the “fresh” reference water is a just a low salinity reference water and is not meant to represent the salinity of the infiltrating water; i.e. these reference waters bound the possible salinity values. All salinity boundary conditions are a mixture of both reference waters.

Most of the calculations carried out in the current project use this simplified approach to salt transport with variant calculations are also carried out using five reference waters and modified boundary conditions for tractability (see Section 4.5).

4.4 Rock properties

The physical properties used in the calculations [detailed in Joyce et al. (2010a)], relating to diffusion, dispersion and matrix diffusion, are shown in Table 4-2 and Table 4-3. Values are consistent between ECPM and DFN calculations. If the property is dependent on rock type, for example the matrix block size, then for a discrete fracture the value specified is determined by the rock type at the centre point of the fracture.

Table 4-2: Diffusion, dispersion and matrix properties for all rock types.

Parameter	Value
Transverse dispersion length	15 m
Longitudinal dispersion length	40 m
Salt diffusion coefficient	1.0×10^{-9} $m^2\cdot s^{-1}$
Intrinsic (matrix) diffusion coefficient	4.0×10^{-15} $m^2\cdot s^{-1}$
Matrix porosity	3.7×10^{-3}

Table 4-3: Matrix block size for each rock type (this defines the maximum distance contaminants can diffuse into the rock matrix). Rock types are used to distinguish between different HRDs and also different depths. Increasing x in the rock name (HRDx) refers to increasing depth.

Rock Name	Matrix Block Size(m)
HRD1R, HRD1L, HRD2R, HRD2L	1.66
HRD3R, HRD3L, HRD4R, HRD4L, HRD1RFFM01, HRD1LFFM01, HRD2RFFM01, HRD2LFFM01, HRD1RFFM06, HRD1LFFM06, HRD2RFFM06, HRD2LFFM06	3.3
HRD3RFFM01, HRD3LFFM01, HRD4RFFM01, RD4LFFM01, HRD4RFFM03, HRD4LFFM03, HRD4RFFM04, HRD4LFFM04, HRD4RFFM05, HRD4LFFM05, HRD3RFFM06, HRD3LFFM06, HRD4RFFM06, HRD4LFFM06	6.5
HRD1RFFM02, HRD1LFFM02, HRD2RFFM02, RD2LFFM02, HRD3RFFM02, HRD3LFFM02, HRD4RFFM02, HRD4LFFM02	1.5
HRD1RFFM03, HRD1LFFM03, HRD2RFFM03, RD2LFFM03, HRD3RFFM03, HRD3LFFM03, HRD1RFFM04, RD1LFFM04, HRD2RFFM04, HRD2LFFM04, HRD3RFFM04, RD3LFFM04, HRD1RFFM05, HRD1LFFM05, HRD2RFFM05, RD2LFFM05, HRD3RFFM05, HRD3LFFM05	5.5

4.5 Initial conditions and boundary conditions

The regional model developed in SR-Site (Joyce et al. 2010a) simulated the past evolution of groundwater composition from 8000 BC to 2000 AD. The timestep at 2000 AD from this regional model is used as the initial state for the calculations presented in the next section.

Figure 4-5 shows the initial salinity at 2000 AD within the fractures, which is interpolated from the regional model salinity. For simplicity, the initial salinity within the rock matrix is assumed to be the same as the initial salinity within the fractures (and thus is also equal to the regional model fracture salinity at 2000 AD). The salinity of the matrix water is expected to slow, to some extent, the penetration of meteoric water.

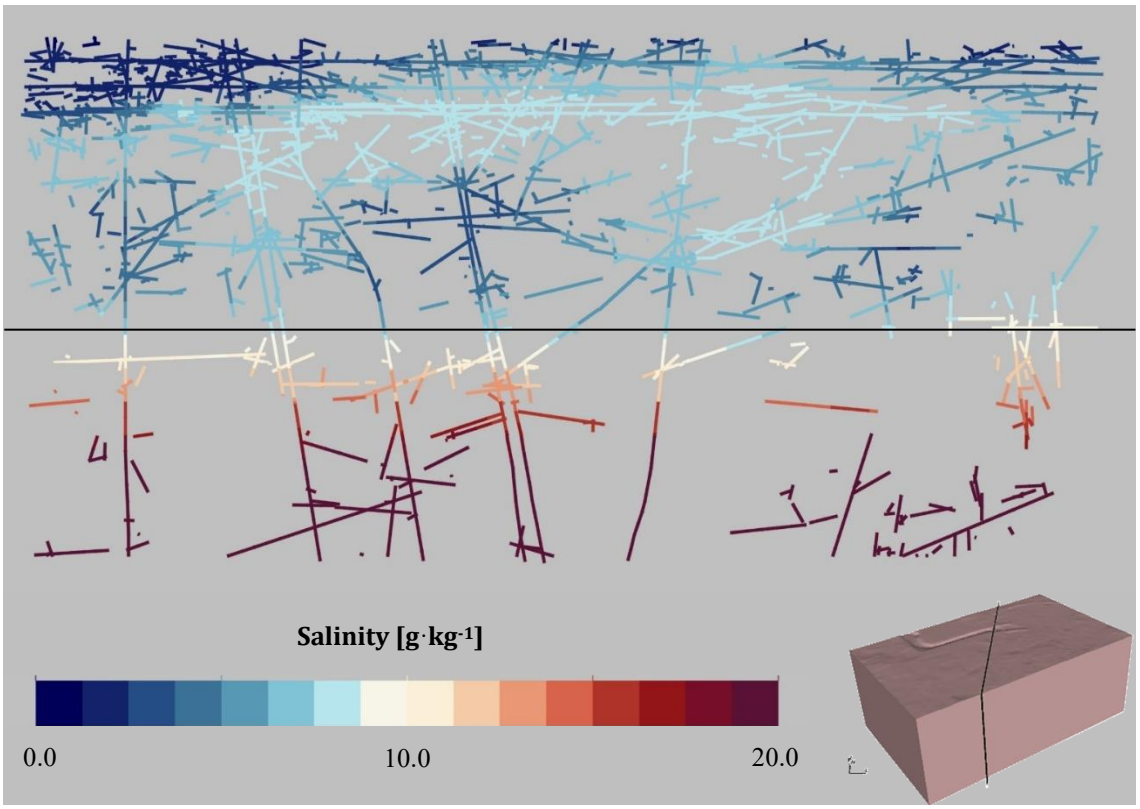

Figure 4-5: *Vertical slices (location shown in bottom right) showing the initial salinity in the fractures and the matrix. The horizontal black line shows the repository depth.*

Dirichlet boundary conditions are used for both pressure and groundwater composition on the top surface of the model. The Dirichlet boundary values are taken from the regional model at 2000 AD and are fixed for the duration of each transient simulation. (Note, the boundary condition for salinity is applied using a mixture of the two reference waters chosen to give the same salinity as the regional scale model. Therefore the salinity boundary condition varies with location; locations on the sea bed, for example, have more of the saline reference water, while locations on land have more of the fresh reference water). Ideally, nonlinear boundary conditions would be used on the top surface that would allow the pressure and water composition to evolve there in a self-consistent manner. Unfortunately, these nonlinear boundary conditions required an unfeasibly small timestep for the current model when tested.

The boundary conditions on the sides and bottom of the model are no-flow for the pressure calculation and no-flux for the transport calculation. This means that all recharge and discharge points are located within the top surface of the model domain (and ensures recharge is composed of dilute surface water). It is recognised that several of the physical recharge and discharge locations may exist outside the model domain (and may also move with time) and that flow would be expected to enter and leave through the lateral surfaces of this domain. However, it was necessary to only allow flow through the top of the model to ensure dilution occurred, in this repository scale model, when using Dirichlet boundary conditions.

The variant calculations that include five reference waters were more computationally demanding. Therefore, different boundary conditions were used, with reference water mass fractions fixed on the bottom and sides of the model. Using these fixed mass fractions means the model reaches steady state more quickly. This is less useful for predicting the expected timescales for salinity evolution but can still be used to compare ECPM and DFN approaches and consider qualitatively the evolution of the groundwater composition under these boundary conditions.

4.6 Upscaling

For the purposes of comparison, an ECPM representation of the model has been created in addition to the DFN. For the ECPM representation, the properties of the fracture network are transferred onto a three-dimensional mesh of hexahedral cells in a process known as upscaling.

In the current project, flow-based upscaling (Jackson et al. 2000) has been used. This process applies pressure gradients across the fracture network within each cell and calculates the flow response from the fractures to determine the permeability of the cell. The kinematic porosity and fracture area per unit volume are calculated trivially from the areas and transport apertures of the fractures within each cell (the fracture area per unit volume is an input for rock matrix diffusion calculations). The properties of planar features such as sheet joints and plane-projected fractures have been represented using the implicit fracture zone (IFZ) method (Svensson 1999) which is distinct from the upscaling method (Jackson et al. 2000).

The ECPM mesh used for these calculations has around 266,000 hexahedral cells of dimension 20 m by 20 m by 20 m. A minimum permeability of 10^{-20} m^2, and a minimum porosity of 10^{-8}, are enforced in the ECPM cells. These limits are numerically necessary to ensure that the ECPM finite elements have non-zero permeability and porosity where there are no (or very few) fractures. It is considered that these limits are sufficiently small that any resulting unphysical connectivity is negligible. Figure 4-6 shows the horizontal component of the permeability tensor and the kinematic porosity.

4.7 Particle tracking and analytic RMD calculations

Particle tracking is a technique whereby massless particles are released into a simulated flow field and the resulting trajectories (pathlines) of the particles are calculated. These particle trajectories are purely advective, unaffected by dispersion or diffusion, and have no impact on the flow field. The pathlines can be used to calculate the destination of contaminants or solutes that are released from source points into a flow field. Alternatively, a technique known as reverse particle tracking can be used to calculate recharge locations for given points in a flow field; this is done by simply reversing the flow velocities and calculating the resulting trajectories.

Particle tracking calculations have been carried out for the DFN model. The pressure and density are fixed at the 2000 AD calculated values for the whole trajectory of each pathline. Pathlines are released from a regular grid of start points at -470 m depth, with 10 particles released per start point.

A significant limitation of advective pathlines is that they are unaffected by rock matrix diffusion, which is known to reduce the effective rate at which contaminants migrate. However, the particle tracking data can be post-processed using analytical techniques to provide more realistic travel times. Such techniques were used in previous groundwater modelling for both Forsmark (Joyce et al. 2010a) and Laxemar (Joyce et al. 2010b); although these assumed an infinite rock matrix and ignored the impact of stagnant zones. Since then, the analytical methods available have advanced.

Mahmoudzadeh et al. (2013) developed a method for incorporating both the effect of a finite matrix and the impact of stagnant water zones of finite extent next to a flowing channel. It also accounts for diffusion into the finite rock matrix from stagnant zones. The calculations in (SKB 2022a) are based on this approach, as described in Section 2.2.2, and we have used the same approach here to estimate the impact of RMD on particle tracking calculations. In particular, the solution equation (2) has been implemented numerically in Matlab (Shahkarami 2024), whereby a numerical inversion of the Laplace solution into real space is performed. The parameters used for this analytic calculation are provided in Table 4-4.

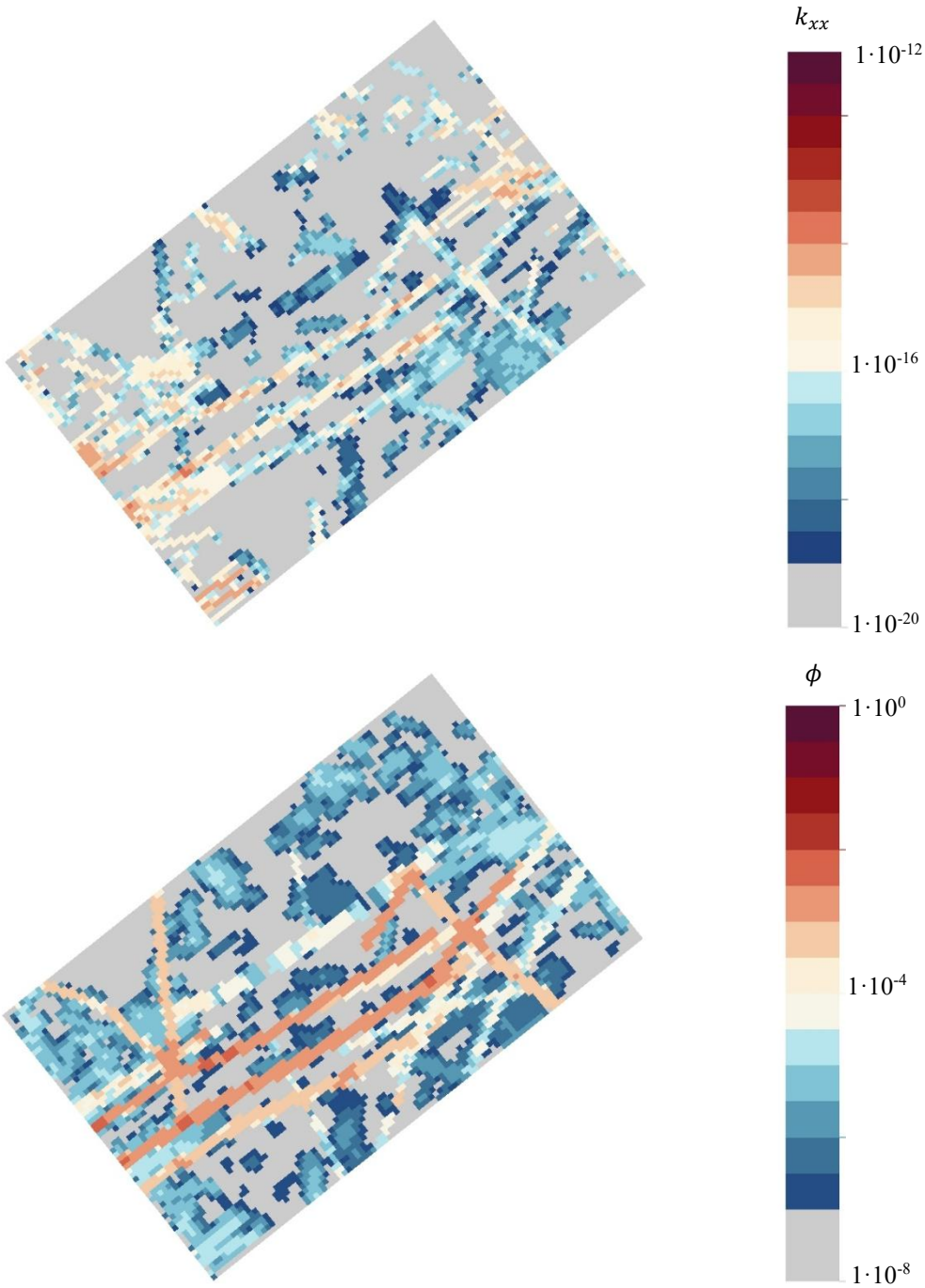

Figure 4-6: *Horizontal slices at 470 m below current sea level. These show the upscaled horizontal component of the permeability tensor (**$\mathbf{k_{xx}}$** top) and kinematic porosity (**$\boldsymbol{\phi}$** bottom).*

Table 4-4: Parameters for pathline and analytic RMD calculations. Values are consistent with those used in the ADE calculations (Table 4-2 and Table 4-3). The matrix depth is appropriate for the volume of rock around the repository. C_0 is equal to the average initial salinity at repository depth taken from the ADE calculations. C_{in} is equal to the effective inlet salinity in the ADE calculations.

Parameter	Value
Initial salinity (C_0)	9.35 g·kg^{-1}
Inlet salinity (C_{in})	1 g·kg^{-1}
Matrix Depth	6.5 m
Intrinsic (matrix) diffusion coefficient	4.0×10^{-15} m^2·s^{-1}
Matrix porosity	3.7×10^{-3}

5 Calculation Results for two reference waters

This section compares DFN and ECPM ADE dilution calculations, using two reference waters, with equivalent 1D pathline transport calculations. This enables an assessment of the limitations of the more approximate ECPM and 1D pathline transport calculations. However, in the first subsection below, an attempt is made to simplify the ADE calculations to understand when good agreement can be achieved between these and the pathline calculations. In the subsections that follow, more complexity is introduced, creating starker contrasts between the different methods.

5.1 Comparison of advective pathlines with advection-dispersion calculations without RMD

In this subsection, additional approximations are made in the advection dispersion calculations to understand when a close match with the pathline calculations can be achieved (and implicitly the converse):

- Rock matrix diffusion is ignored in the advection-dispersion calculations and is not applied to pathlines as a post-processing step.
- The flow solution is held constant from the first timestep and does not evolve self-consistently with the salinity. The salinity therefore effectively transports like a tracer.

Reverse pathlines were initiated from a regular grid of points at -470 m. Ten particles are attempted for each grid point, with the exact start point of each constrained to be on fracture intersections within 30 m of the grid point. The starting intersection is chosen randomly but the probability of starting on a given intersection is weighted according to the flux through the intersection (with greater weighting for greater flux). Reverse pathlines that do not reach the surface, or do not have a valid start point, are ignored. Figure 5-1 shows the pathlines, their start points at repository depth, and their endpoints (recharge locations). Start point locations are biased towards features with greater flow due to the flux-weighting, although this was not found to have a strong impact on the final results.

Figure 5-1 indicates that the recharge points (blue) are mostly to the south and near the model boundary. (The recharge points shown are those that successfully connect to repository depth in the pathline calculations; there may be other recharge points, not shown, that either connect to shallower locations or were not included due to numerical issues). The proximity of the recharge points to the boundary suggests that the repository scale model domain is likely too small to capture all of the physical recharge points of the system (as discussed in Section 4.5). It is recognised that this could qualitatively influence dilution times but the model should nonetheless be suitable for comparing the different methodologies.

Many pathlines dip below the repository between the repository and the recharge points. These pathlines indicate that there are upflows of water at some locations (fracture intersections) at repository depth. Given that the salinity is greater below the repository, salinity may therefore temporarily increase at those locations before dilution occurs (this is confirmed in Section 5.4).

The total time taken for each pathline to reach the surface of the model is recorded and used to calculate an average salinity at repository depth. The assumed average salinity, $C(t)$, at time t is calculated using:

$$C(t) = C_0 + (C_{in} - C_0)\frac{n(t)}{N} \tag{5.1}$$

where C_0 is the initial average salinity at repository depth, C_{in} is the average inflow salinity, $n(t)$ is the number of reverse pathlines reaching the surface as a function of time, and N is the total number of reverse pathlines reaching the surface. The values of C_0 and C_{in} are given in Table 4-4, and $C(t)$ is plotted in Figure 5-2.

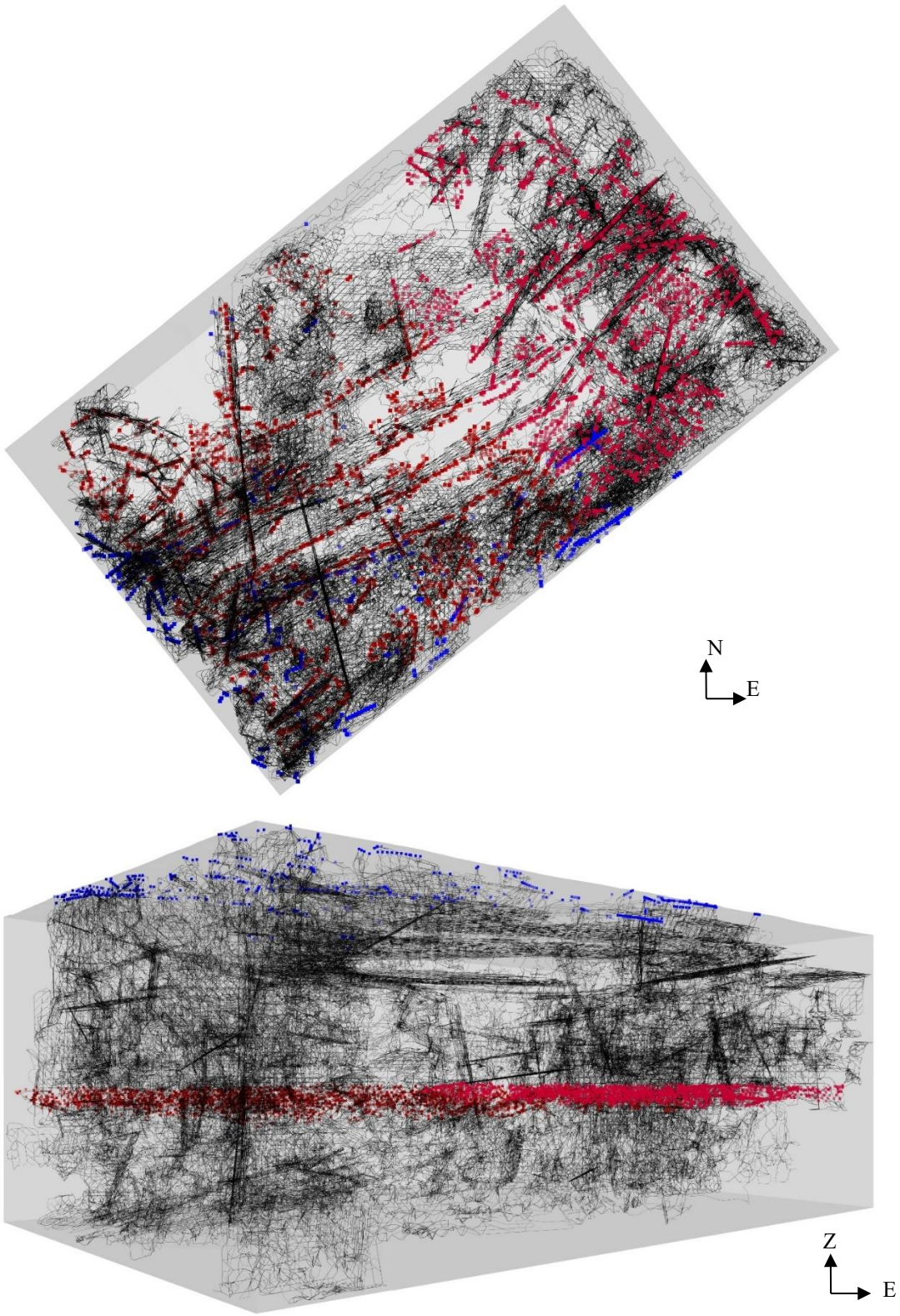

Figure 5-1: *DFN reverse pathlines (black) started on intersections at repository depth. The exact start points are indicated in red while the end points (recharge locations) are indicated in blue.*

The advection dispersion equations are solved transiently for a period of 100,000 years, starting at 2000 AD. As time progresses the saline water at repository depth is steadily displaced by fresh water originating from the recharge locations within the model. It is emphasised that the ADE calculation assumes a static flow field (calculated at 2000 AD) which is the same as that used in the particle tracking calculations.

Figure 5-2 plots the average salinity of salt at repository depth for each of the different calculation methods. For the DFN ADE method, the average is taken over all fracture intersections between depths of -465 and -475 m. For the ECPM ADE method, the average is taken over all nodes at the same depth interval, but excluding those with very low permeabilities, so that only nodes nearby to fractures are included. Pathline "salinities" calculated using equation (12) are also plotted. The pathline calculations predict quicker dilution than the DFN or ECPM ADE calculations. This is partly because the initial condition for the advection-dispersion calculation has greater salinity at depths below the repository which means some of the recharge pathways travel down below the repository before rising to repository depth (Figure 5-1). This initially pushes through additional salinity before the dilute water arrives, and therefore delays the dilution process (on average). The increase in salinity is only just apparent for the average salinities plotted in Figure 5-2, because not all flow paths exhibit this behaviour, but it is much clearer when looking at individual release points (see Section 5.4).

A modified DFN advection dispersion calculation is also presented in Figure 5-2. In this case the initial salinity is uniform and does not increase with depth (although the flow field is kept the same). The values of C_0 and C_{in} match those used for the pathline calculations (see Table 4-4). For this case the dilution process proceeds more rapidly and in closer agreement with the particle tracks.

Comparing the ECPM and DFN advection dispersion calculations, dilution progresses more slowly for the ECPM. This is thought to be because the ECPM calculation routes more flow below repository depth, thus pushing through more salinity initially and slowing the dilution process. This is emphasised by the fact the average salinity for the ECPM case very slightly increases at repository depth between 100 and 1000 years after present. Note that ECPM cells are 20 m in dimension and thus may include several flowing DFN features and several reverse pathline start points. As such, the results for each ECPM cell will represent an "average" of the distribution of DFN dilution times within it.

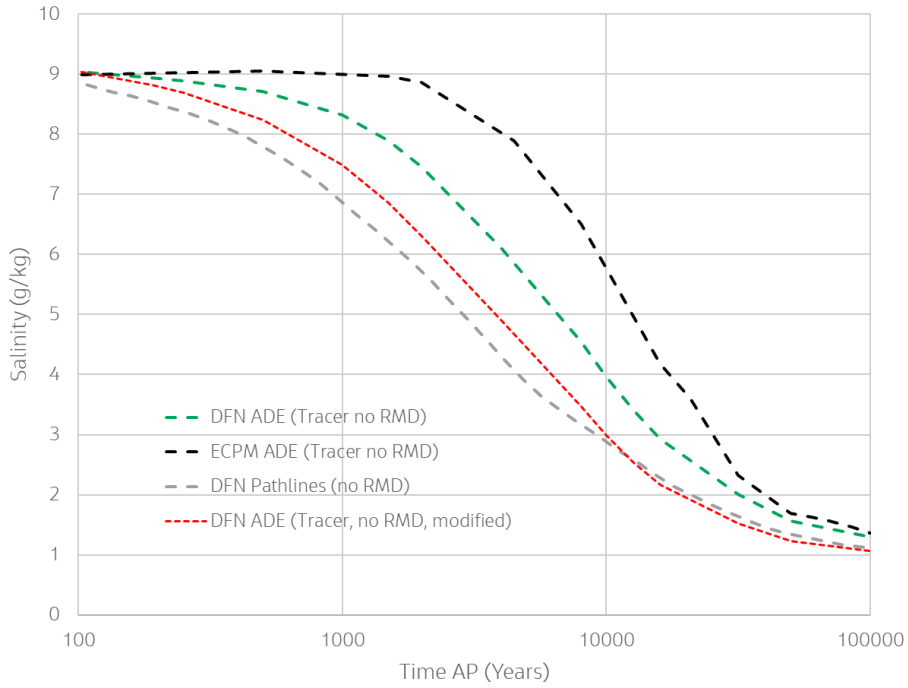

Figure 5-2: *Comparison of salinities predicted by ECPM and DFN advection-dispersion equation (ADE) tracer calculations with those from an advective pathline calculation. The "modified" DFN calculation has an idealised top boundary condition and initial condition that better match the assumptions made in the pathline salinity calculation.*

5.2 Comparison of advective pathlines with advection-dispersion calculations using RMD

In this section, rock matrix diffusion (RMD) is explicitly included in the ECPM and DFN advection dispersion (ADE) calculations, as well as in the advective pathline calculations using the analytic approach described in Section 4.7. All the ADE calculations use tracer transport, where the density and flow fields remain static (as was the case for the calculations without RMD in Section 5.1).

Figure 5-3 shows the evolution of the average salinity at repository depth for various transport models. Calculations using ECPM and DFN ADE with RMD are compared with predictions made using DFN advective pathlines including analytic RMD. For reference, equivalent calculations without RMD are displayed on the same axes. Pathline calculations predict faster dilution than the equivalent ADE calculations (as was the case when RMD was excluded) but have a reasonable match at later times. It is expected that the main reason for the difference is because the pathline calculations, with only 10 sampled paths per release point, are unable to fully incorporate mixing that occurs along the flow path. Comparing the dilution rates predicted by ECPM and DFN ADE calculations, the ECPM predicts faster dilution by a factor of 2-3. Therefore, the pathline and ECPM models are cautious by predicting more rapid dilution that the full DFN ADE calculations.

Considering the ECPM and DFN ADE calculations in more detail, it is apparent that the ECPM with RMD predicts faster dilution than the equivalent DFN calculation, while the ECPM without RMD predicts slower dilution than the equivalent DFN calculation. Thus, it appears that RMD is having a stronger impact on the DFN ADE calculations than the ECPM ADE.

Figure 5-4 and Figure 5-5 show horizontal slices through the DFN and ECPM models (including RMD), at repository depth, for six timesteps. As the simulation progresses the salinity distribution at repository depth evolves. After 1000 years, the salinity in some places has reduced, but in others it has increased. The increase in salinity in certain locations is due to flow initially travelling below the repository before flowing back up to repository depth. However, as time progresses, both the ECPM and DFN models show more and more dilution until almost complete dilution is achieved.

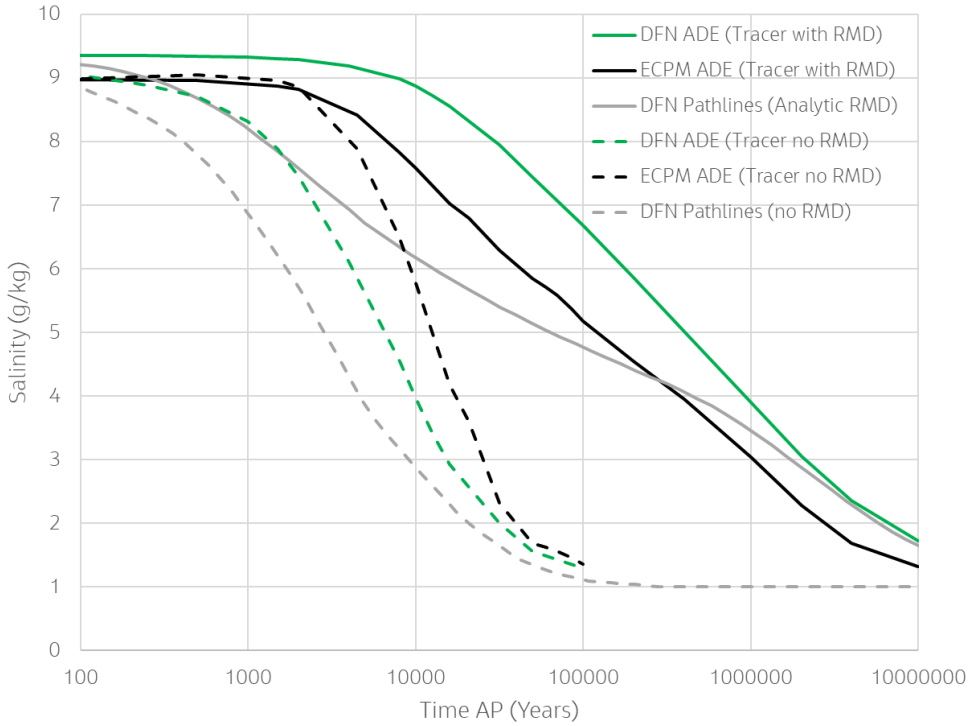

Figure 5-3: *Salinity plotted as a function of time for various transport models. Dashed lines indicate calculations without RMD while solid lines denote those with RMD. The advection diffusion (ADE) calculations assume a static density/flow field and are effectively tracer calculations. The salinities calculated using DFN pathlines with analytic RMD use equation 2 and salinities calculated using DFN pathlines without RMD use equation 12.*

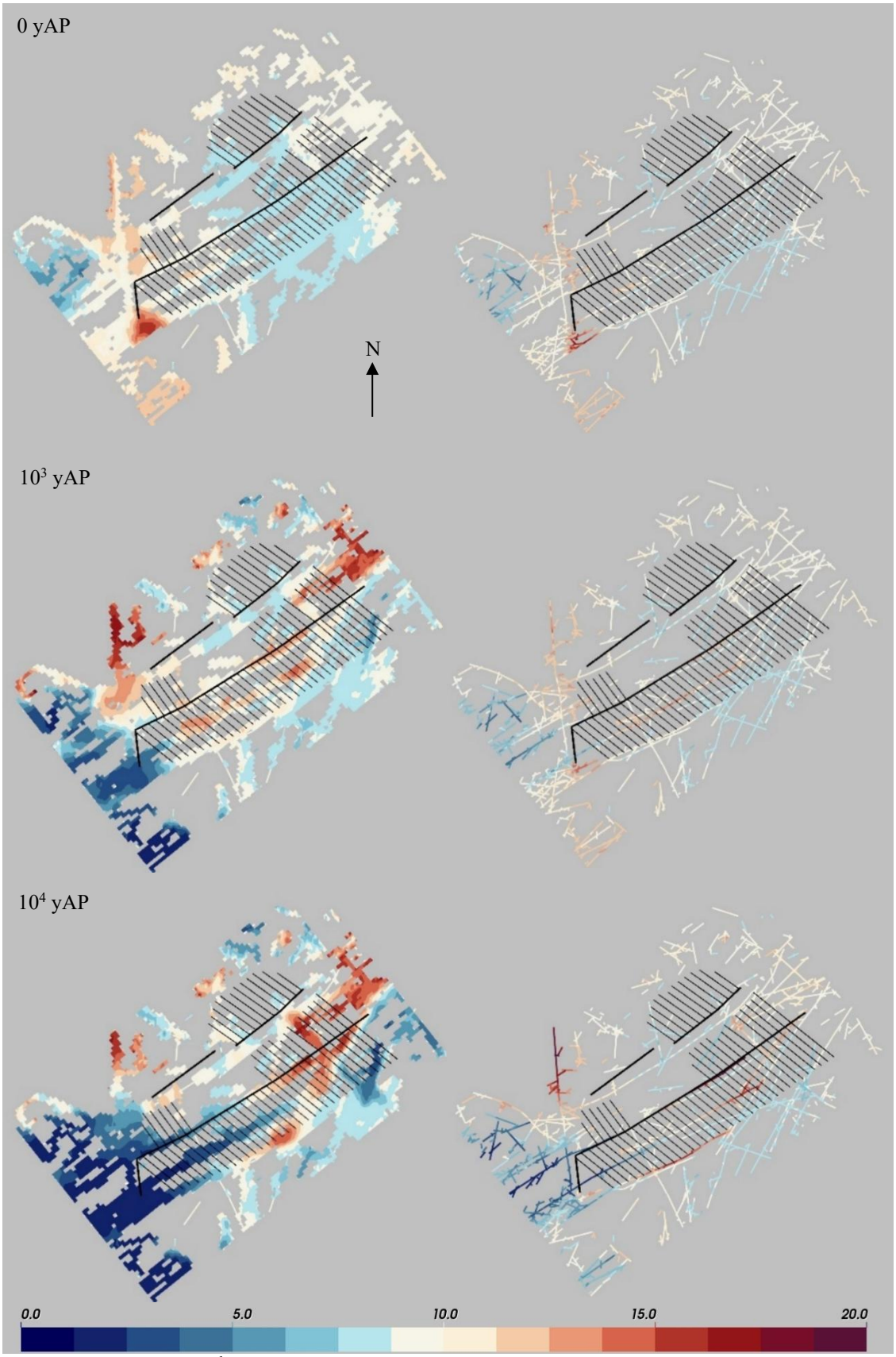

Figure 5-4: *Salinities (g·kg^{-1}) for a horizontal slice at -470 m elevation. The ECPM representation (left) and DFN representation (right) are compared for 3 times. Continued in Figure 5-5.*

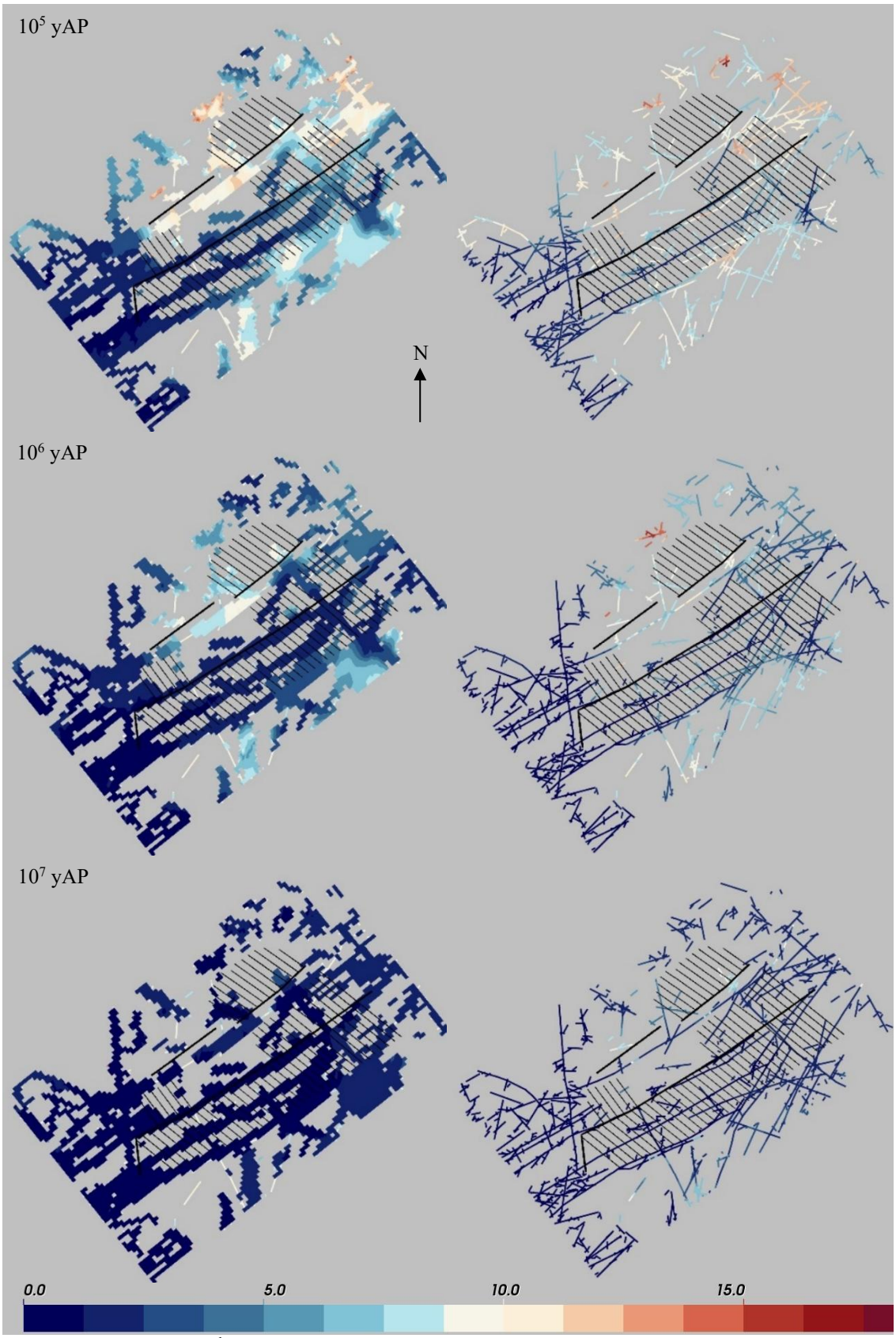

Figure 5-5: *Salinities (g·kg^{-1}) for a horizontal slice at -470 m elevation. The ECPM representation (left) and DFN representation (right) are compared for 3 times. Continued from Figure 5-4.*

5.3 The impact of coupling flow and salinity

In Sections 5.1 and 5.2, the DFN and ECPM advection-dispersion calculations assumed the pressure and density remained constant throughout the simulation. This meant the solutes were effectively treated as tracers and the changing salinities did not feed back into the flow solution via the buoyancy term. In this section, variant ECPM and DFN calculations have been carried out which relax this assumption and fully couple together the solution of the flow and solute transport calculations. These coupled calculations are numerically very challenging and were carried out for a shorter period of 100,000 years.

Figure 5-6 shows the results of these coupled calculations and compares them against the equivalent calculations where the constant pressure assumption was made. It is apparent that after several thousand years, for both the DFN and the ECPM calculations, the rate of dilution for the coupled calculations is slower than the tracer calculations. From the perspective of dilution, using the tracer approximation appears to be a conservative assumption (in this case). It is not clear why – it is possible the initial flow field used for the tracer calculations produces shorter flow paths than the evolved flow field resulting from lower salinity.

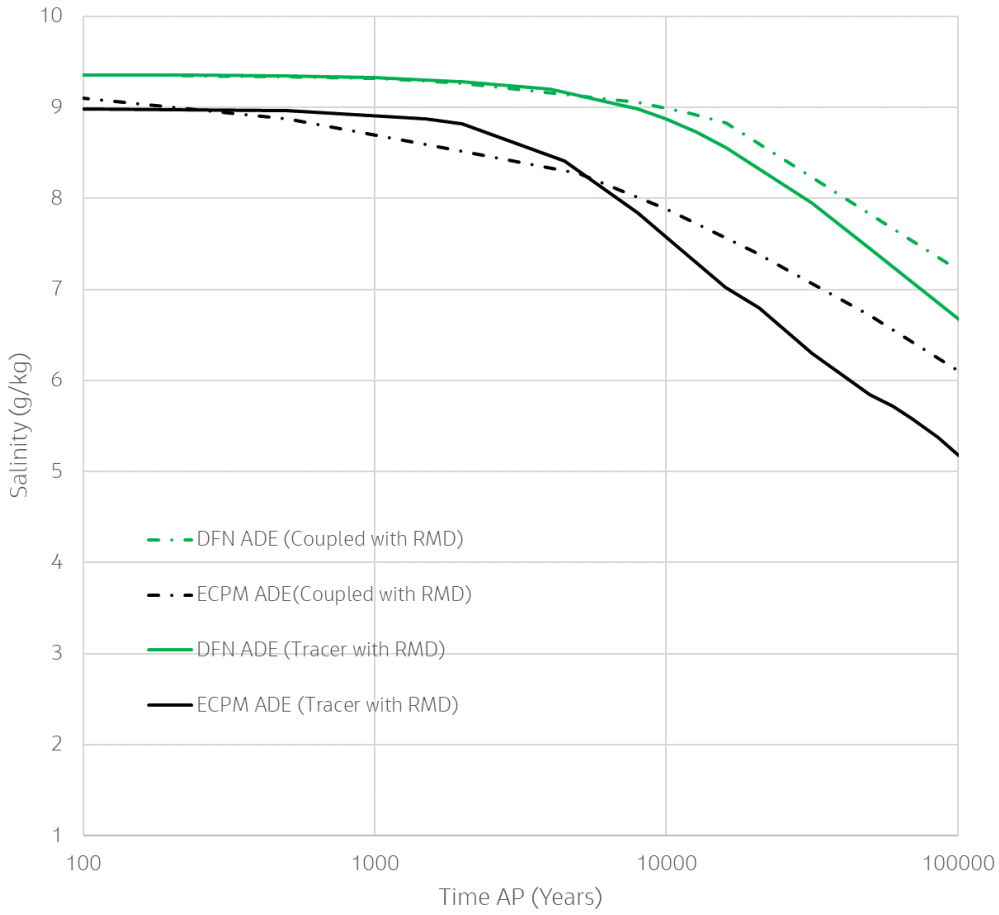

Figure 5-6: *Comparison of different advection-dispersion calculations. The solid lines denote tracer calculations where the flow field remains static. The dashed lines denote fully coupled calculations where the evolving salinity impacts the density and thus the flow field.*

5.4 Comparisons at specific locations

This section compares the salinities from DFN ADE calculations (tracer calculations with static flow fields and including RMD) versus those from pathlines with analytic RMD. Figure 5-7 shows the four locations chosen to make these comparisons; these locations are at fracture intersections near to the repository tunnels (engineered features that are not explicitly modelled). Ten reverse pathlines are released from each location, with the analytic RMD method applied, as described in Section 4.7. The resulting salinities are plotted against the ADE salinities at the same intersections in Figure 5-8.

The DFN ADE salinity initially increases for points (b) and (c), before reducing, while for points (a) and (d) there is a consistent reduction in salinity. On careful examination, this is consistent with the slices seen in Figure 5-4. The initial increase in salinity for points (b) and (c) is due to saline water being pushed up initially from beneath. (It is interesting that (a) doesn't see this effect given its proximity to (b), demonstrating the structural control effect from the fracture network). The pathline calculations assume a constant initial salinity within the fractures and therefore do not show this behaviour. The dilution predicted by the pathline calculations typically occurs more quickly than predicted by the ADE calculations, which is consistent with the average behaviour shown in Figure 5-3. Also note that there is a significant spread in the particle tracking results at each location, which occurs despite a flux weighting for the pathline start points. This indicates a high degree of dispersion, presumably generated by the structural controls within the DFN.

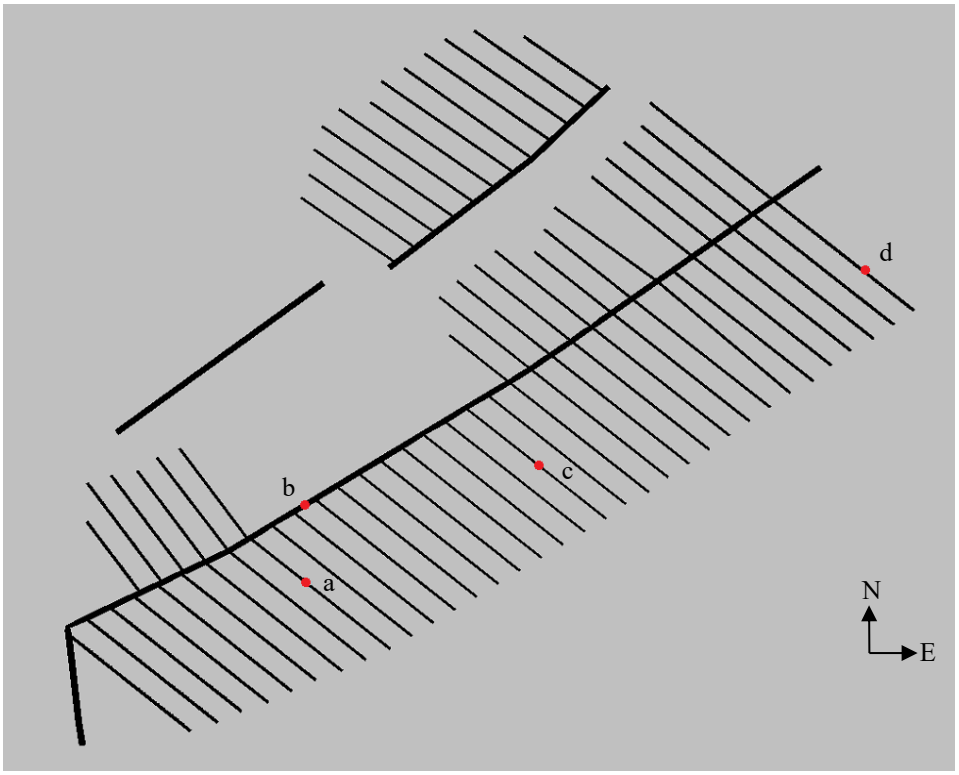

Figure 5-7: *The four release locations (a, b, c and d) used for the comparisons in Figure 5-8 relative to engineered tunnels. Note that the engineering is not explicitly modelled.*

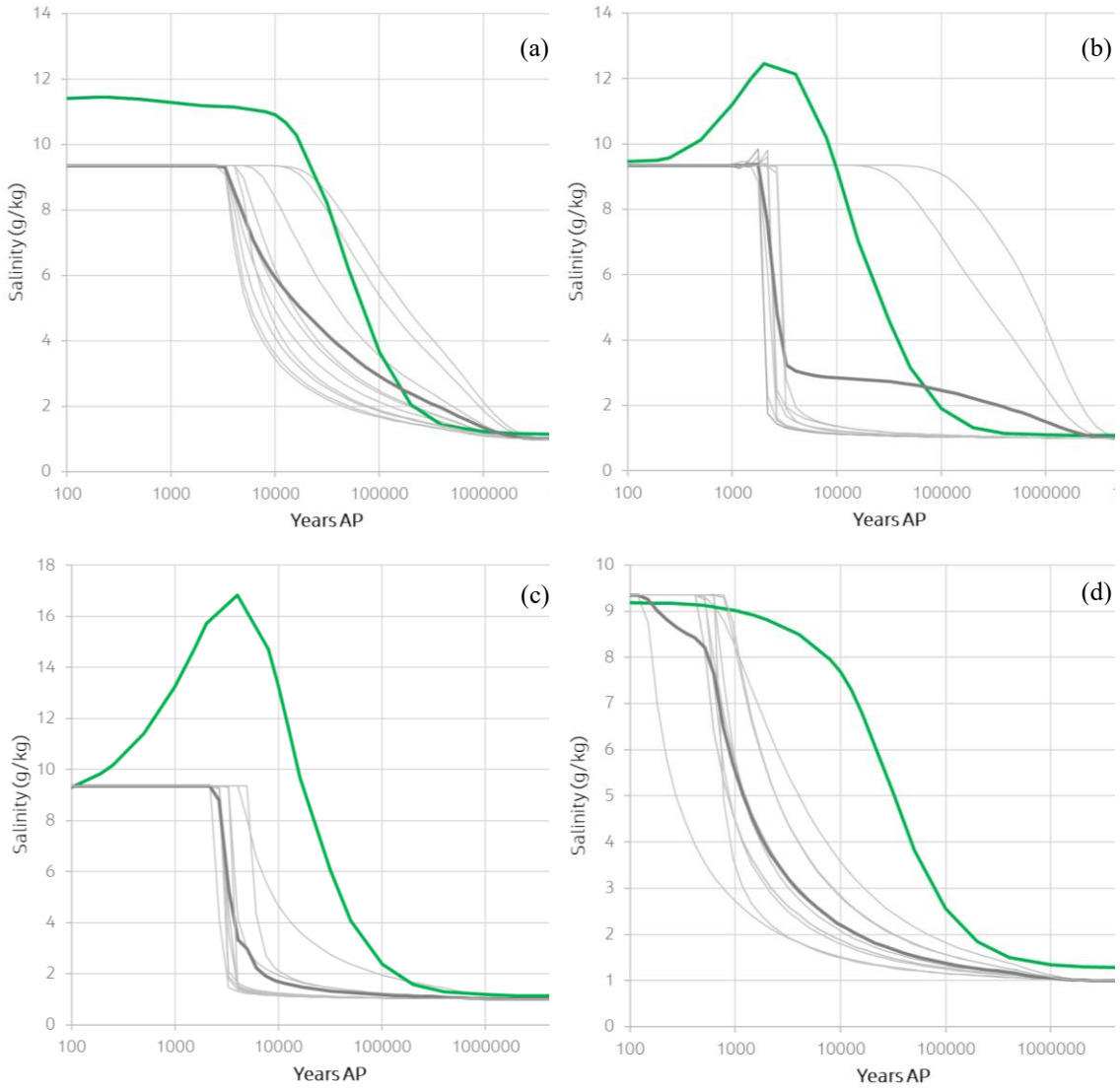

Figure 5-8: *Comparison of DFN ADE salinities (green) versus pathlines with analytic RMD (grey) calculated using equation (2). The thin grey lines represent the salinities from the 10 particles released from each location and the thick grey line is the average of the 10 pathline salinities. The four plots correspond to the four locations specified in Figure 5-7.*

6 Five reference water calculations

This section presents DFN and ECPM ADE calculations for five reference waters rather than for two reference waters, as was the case in Section 5. There are three further differences when compared with the two reference water calculations:

- The boundary conditions have been modified, with Dirichlet boundary conditions (for pressure and concentration) applied to every surface of the model (with values taken from the SR-Site regional scale model).
- The solute transport and pressure calculations are fully coupled, with changes in salinity modifying the pressure via the buoyancy term in the groundwater flow equations (like the variant case in Section 5.3).
- The initial condition in the matrix is captured from the regional scale SR-Site model; rather than assuming the matrix and fracture pore waters have the same composition, as was assumed in the two reference water calculations.

These calculations are designed to provide a comparison of solute transport using DFN and ECPM methods, with as much physical detail as possible. The main limitation comes from the boundary conditions which quite quickly push the system into a steady state equilibrium and so the calculated concentrations will become less physical as time progresses (a short simulation period is also necessary for these computationally challenging calculations). Note that the application of Dirichlet boundary conditions to the sides/bottom of the model allows flow through those faces; therefore, some of the surface recharge and discharge locations are not captured within the domain.

Figure 6-1 shows the mass fraction of brine, at repository depth, for ECPM and DFN calculations, at selected time steps. There are some moderately high mass fractions of brine to the east in the model which dissipate, to some degree, as the simulation evolves. The brine mass fraction also reduces towards the west of the model. Conversely (but only in the ECPM calculations), the mass fraction increases with time along some of the deformation zones that stretch from the south-west to the north-east. The brine is assumed to have travelled upwards from beneath the repository.

Figure 6-2 shows the mass fraction of the Littorina reference water, at repository depth, for ECPM and DFN plane-projected deformation zone calculations, at selected time steps. The mass fraction increases as the simulation progresses, with the Littorina reference water appearing to travel in from the western boundary, particularly along the deformation zones. The ECPM and DFN representations have very similar behaviour, the main difference being at two locations to the east where the mass fraction increases more quickly in the DFN.

Figure 6-3 shows the mass fraction of meteoric water, at repository depth, for ECPM and DFN plane-projected deformation zone calculations, at selected time steps. A logarithmic scale has been used for the mass fractions in this case to show areas where the meteoric reference water is present, even at low mass fractions. Throughout the simulation, the mass fraction of the meteoric reference water is largest in the west, with a lower mass fraction in the east and very low mass fractions elsewhere. As time progresses the meteoric reference water is increasingly present towards the middle of the model. In the DFN model, the meteoric reference water also significantly increases in mass fraction to the east as time progresses, which is not so pronounced in the ECPM model. This is a clear indication that the structural controls within the DFN calculation are producing different localised results, as one might expect.

Figure 6-4 shows the mass fraction of the glacial reference water, at repository depth, for ECPM and DFN plane-projected deformation zone calculations, at selected time steps. At the start of the simulation the mass fractions are low in most areas with a few areas with higher mass fractions (which are more notable in the ECPM). These areas with high mass fractions are where there are no fractures in the ECPM. As time progresses, the higher mass fractions dissipate, except for a small region to the north-west, which is attached to a boundary. The mass fraction cannot reduce significantly there because it is held fixed by the boundary condition.

Figure 6-5 shows the mass fraction of the old meteoric reference water, at repository depth, for ECPM and DFN plane-projected deformation zone calculations, at selected time steps. This is the dominant reference water component at repository depth in most areas. As time progresses the mass fraction of the old meteoric reference water decreases notably, from the west. In the DFN simulation, the mass fraction also decreases in some areas to the east.

Overall, the ECPM and DFN calculations provide similar behaviour but there are some notable differences as well. For the DFN, but not the ECPM, there are some areas to the east where the mass fractions of the old meteoric reference water and the brine reference water decrease with time, while the mass fractions of the meteoric and Littorina reference waters increase with time. The difference between DFN and ECPM cases is probably due to changes in connectivity brought about by the upscaling process.

Due to the different boundary conditions used in the two and five reference water cases it is not possible to directly compare the results. However, some qualitative observations can be made. Firstly, it is apparent from both calculations (Figure 5-4 and Figure 6-1) that deeper saline water emerges in some locations (fracture intersections), at repository depth, after a thousand years or so. Secondly, both models (Figure 5-4 and Figure 6-3) show dilution at repository depth occurs first in the west, and then also in a few locations to the east, with the latter more apparent in the DFN calculations. The five reference water calculations identify the dilute water as being meteoric in origin.

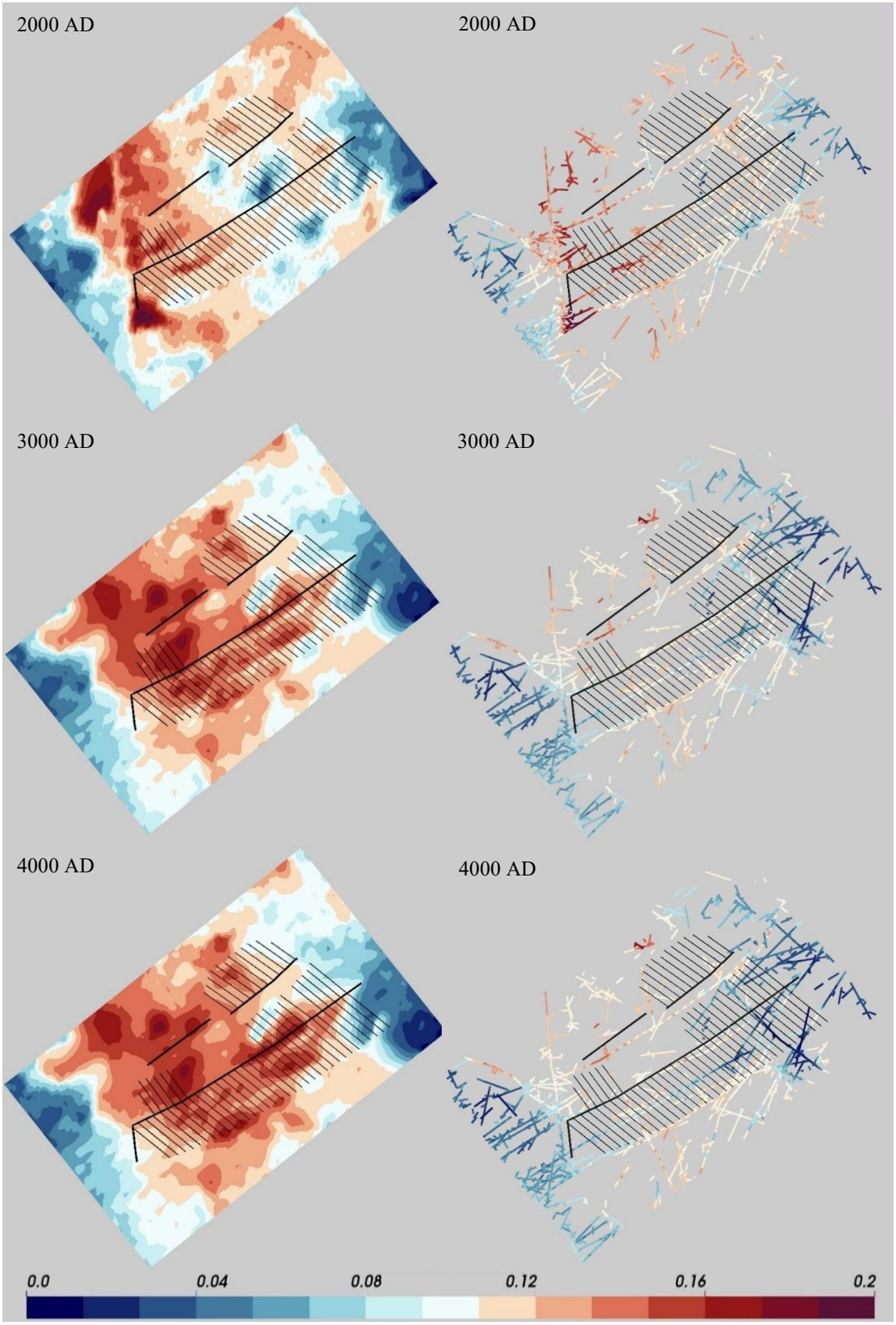

Figure 6-1: *Mass fraction for brine calculated for a horizontal slice at -470 m depth. On the left is the ECPM representation and on the right is the DFN representation. Three timesteps are shown.*

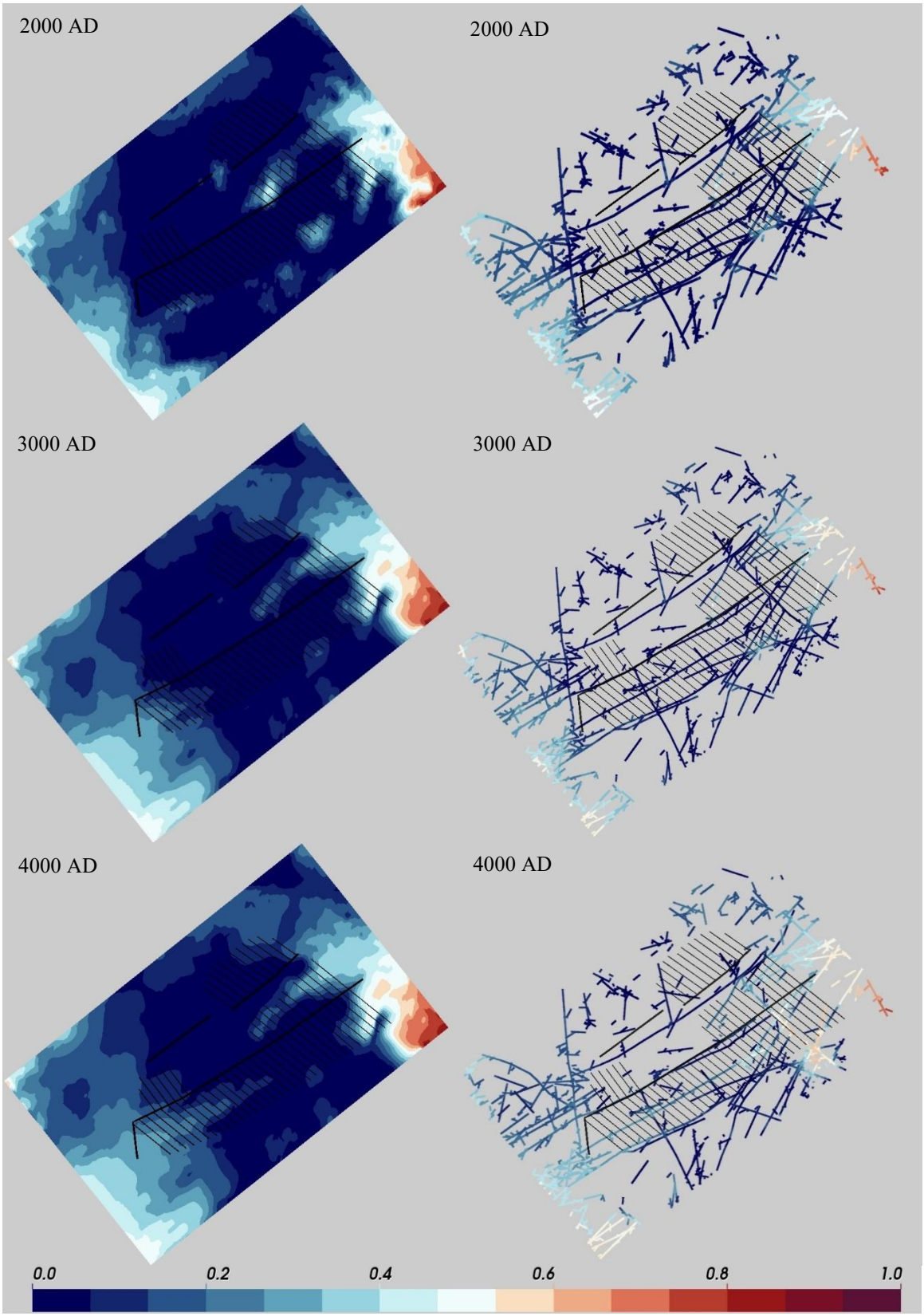

Figure 6-2: *Mass fraction for Littorina water calculated for a horizontal slice at -470 m depth. On the left is the ECPM representation and on the right is the DFN representation. Three timesteps are shown.*

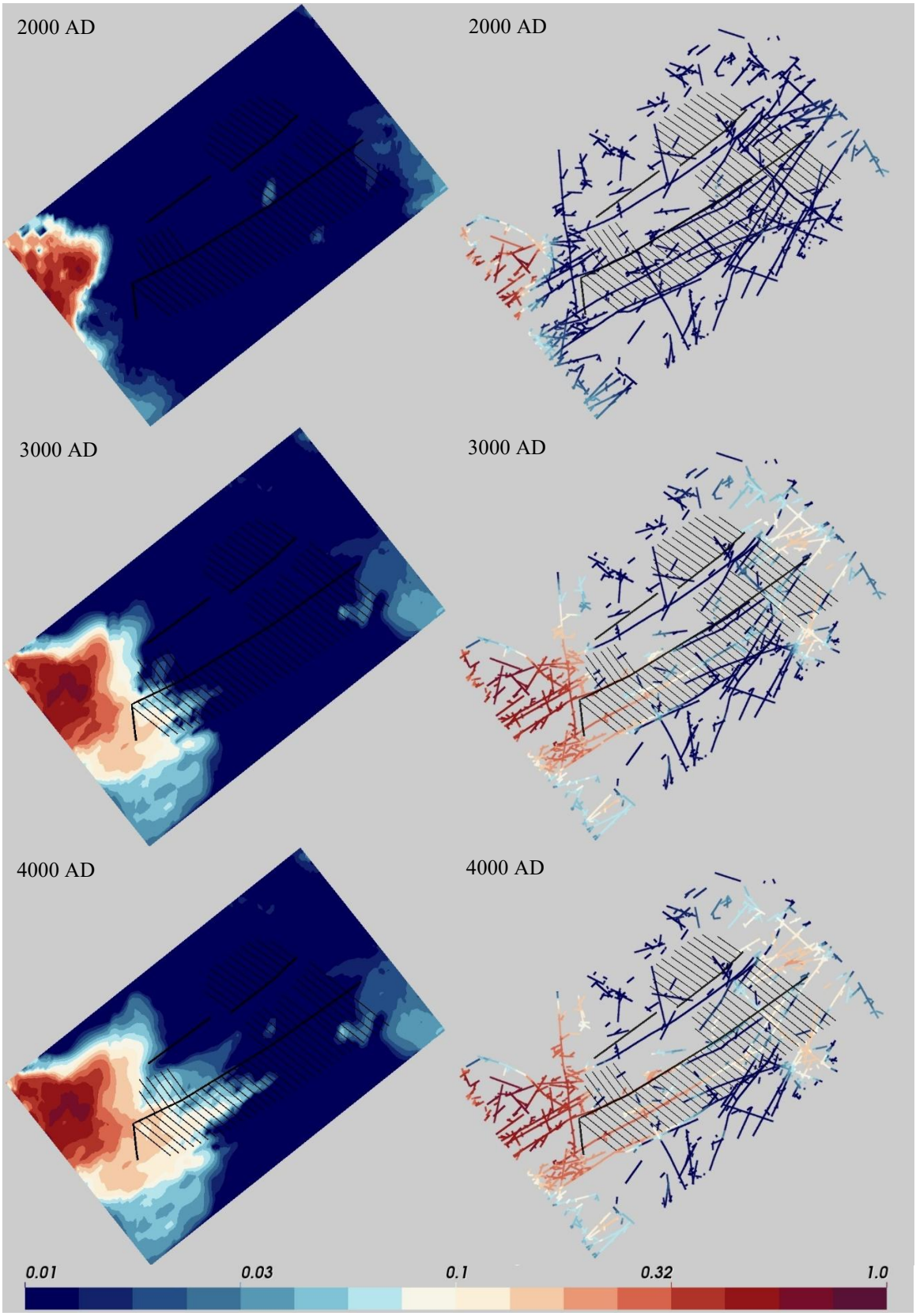

Figure 6-3: *Mass fraction for meteoric water calculated for a horizontal slice at -470 m depth. On the left is the ECPM representation and on the right is the DFN representation. Three timesteps are shown and a logarithmic scale is used.*

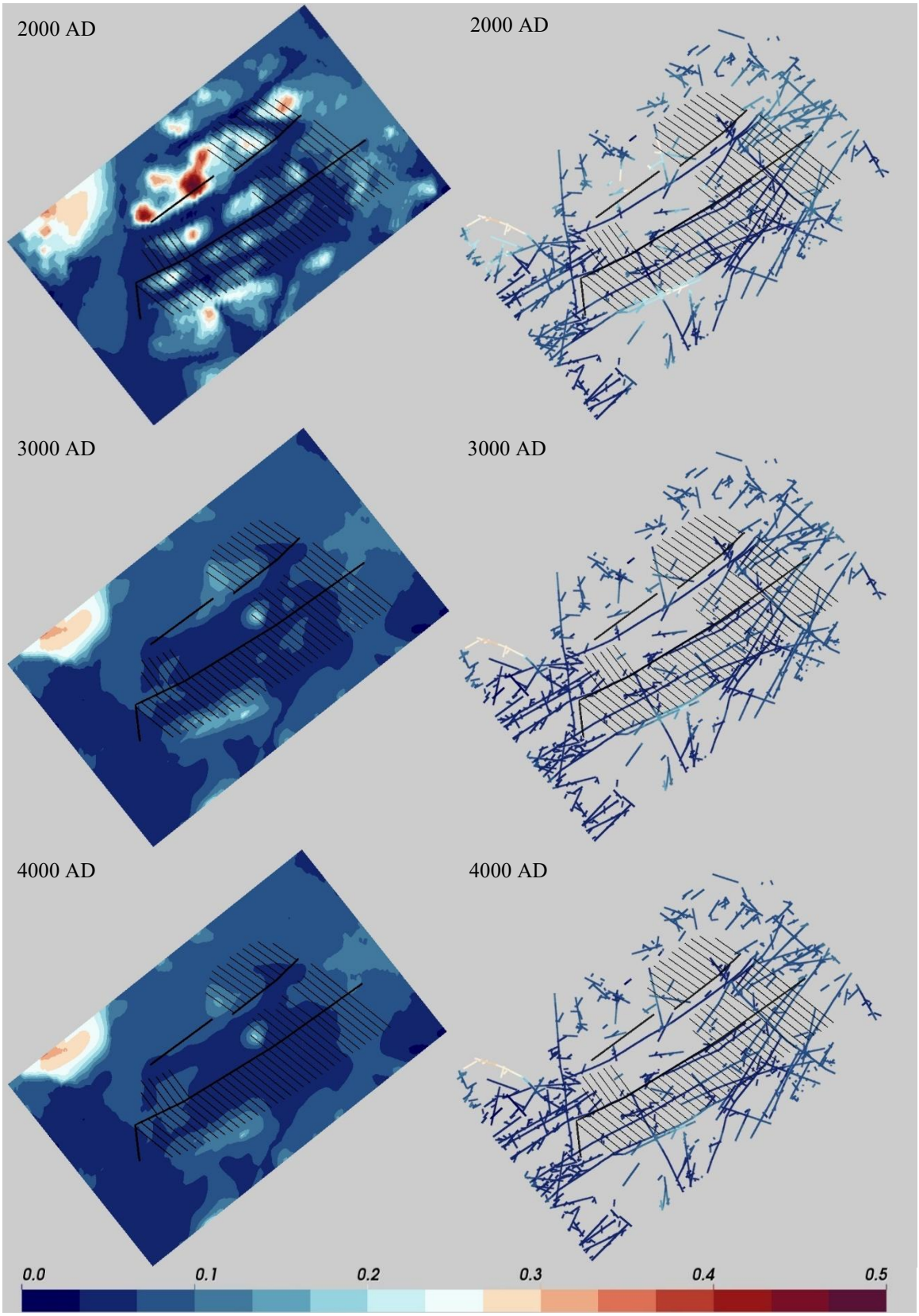

Figure 6-4: *Mass fraction for glacial water calculated for a horizontal slice at -470 m depth. On the left is the ECPM representation and on the right is the DFN representation. Three timesteps are shown.*

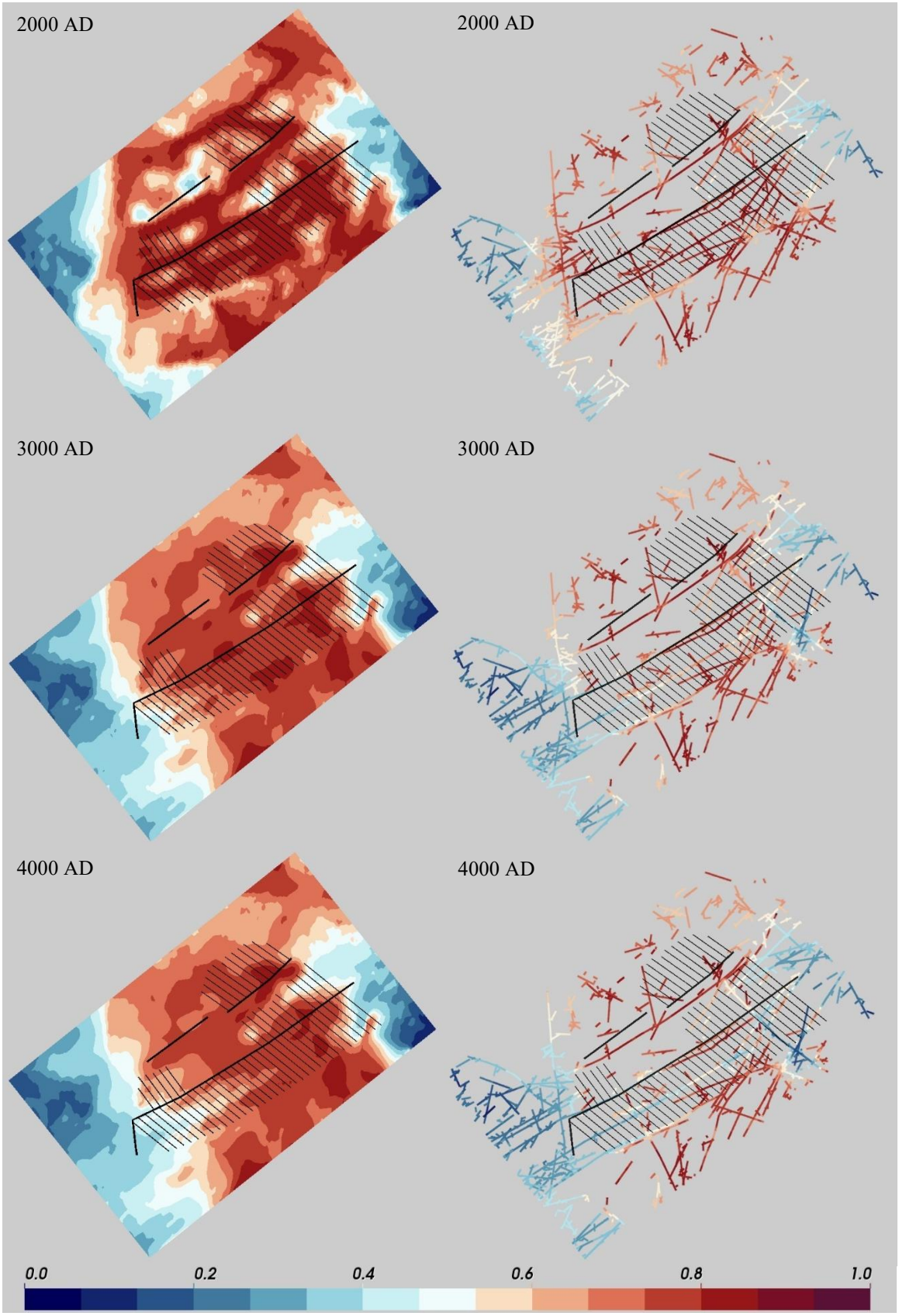

Figure 6-5: *Mass fraction for old meteoric water calculated for a horizontal slice at -470 m depth. On the left is the ECPM representation and on the right is the DFN representation. Three timesteps are shown.*

7 Conclusions

The composition of repository groundwater is a key consideration for SKB's KBS-3 disposal system. SR-Site (Joyce et al. 2010a) included simulations of the evolution of the groundwater composition at Forsmark over a ten-thousand-year period up to the present day and then into the future. These calculations used a regional scale model and an ECPM representation, and the results were calibrated against current day measurements of groundwater composition.

In this report, the groundwater composition at 2000 AD (as simulated in SR-Site) has been used as an initial condition for illustrative calculations that predict and compare the future evolution of the groundwater composition at repository depth using different simulation methods. The calculations are illustrative due to a truncated repository block-scale simulation domain, which does not include all recharge or discharge locations for the repository. The calculations assume that Holocene climatic conditions and present-day sea levels persist. During this period, meteoric water gradually infiltrates to repository depth, altering the groundwater composition within the host rock. Three separate simulation techniques have been used and compared:

- ECPM simulations of saline transport using the advection-diffusion equations (ADE), with and without rock matrix diffusion (RMD).
- DFN ADE simulations of saline transport, with and without RMD.
- DFN based particle tracking simulations using an advective flow field calculated within the DFN at 2000 AD. These calculations include variants with and without an analytical representation of rock matrix diffusion.

The fracture model used in this work has a plane-projected representation of the deformation zones. The ADE calculations use three methods for the representation of salinity:

- Calculations with two reference waters (fresh and saline) in which the transported waters are treated as tracers. The salinity is held fixed at the surface with zero flux boundary conditions on the sides and bottom of the model. The salinity can thus evolve on those latter surfaces.
- Calculations with two reference waters (fresh and saline) in which the transported waters are coupled to the flow field via the evolving density field. These calculations are otherwise equivalent to the tracer calculations.
- Calculations with five reference waters, each water representing the infiltrating water from a different climatic epoch, in the style of SR-Site. The calculations are coupled, with the density and flow fields evolving with the salinity. The salinity is held fixed on all faces of the model. These calculations are computationally more challenging than calculations with two reference waters and have a shorter simulation period.

The two reference water tracer calculations with matrix diffusion show qualitative agreement between the ECPM ADE, DFN ADE and DFN pathlines; all show dilution increasing with time at repository depth, with the pathline-based calculations predicting the fastest dilution, the ECPM predicting slower dilution, and the DFN ADE calculations predicting the slowest dilution. Considering the results in more detail, some locations initially experience an increase in salinity, which is due to the recharge pathways travelling below repository depth, where the water is more saline. This behaviour is only seen in the ADE calculations since the pathline calculations assume a constant initial salinity distribution. As a result, pathline calculations with analytic RMD show faster dilution than the ADE methods. ECPM and DFN ADE calculations show reasonable agreement, but with the ECPM ADE calculations indicating somewhat faster dilution.

The fully coupled two reference water calculations show that coupling flow and transport moderately reduces the rate of dilution (in this case). This may be because the dilution gradually reduces buoyancy effects, enabling percolation to greater depths and increasing the length of some flow pathways.

The calculations with five reference waters include more detail, enabling the future composition of the groundwater to be predicted, rather than just the salinity. The five reference water calculations are not comparable to the two reference water calculations due to the use of different boundary conditions (partly for performance reasons).

The ECPM and DFN calculations with five reference waters exhibit similar behaviour with meteoric water mass fractions clearly increasing over time at repository depth. However, there are some notable differences. For example, in the DFN, but not the ECPM, there are some areas to the east where the mass fractions of the old meteoric and brine reference waters decrease with time, while the mass fractions of the meteoric and Littorina reference waters increase with time. The differences between DFN and ECPM cases are likely attributable to changes in hydraulic connectivity and porosity brought about by the upscaling process.

8 Significance and Recommendations for Future Work

Pathline methods are becoming increasingly sophisticated, allowing them to capture the discrete geometric effects of the fracture network; simulate diffusion into the matrix and stagnant zones of fractures (Mahmoudzadeh et al. 2013); and approximate dispersion via the release of ensembles of pathlines (SKB 2022b). These pathline methods are also more tractable than ECPM or DFN ADE calculations, thus providing a convenient choice for assessing meteoric dilution, especially given their tendency to provide a conservative estimate for dilution timescales. However, these methods do have limitations; mixing and dispersion are not represented explicitly as in ADE-based approaches, the initial variation in solute concentration within the fracture network is not included (SKB 2022b), and flow and transport are not coupled through density-driven effects.

ECPM-based calculations address several of these issues. In particular, they provide an explicit representation of advection-dispersion processes and allow for coupling between flow and transport. However, they do not explicitly resolve flow and transport at the scale of individual fractures and fracture intersections - features known to be important for solute migration in crystalline rock (pathlines calculated within a DFN do take account of these structural controls). Increasing the spatial resolution of the ECPM grid can mitigate this limitation but at greater computational expense. Overall, ECPM calculations require significantly more computational resource than pathline-based methods.

The current work demonstrates a third option for calculating repository water dilution, using explicit DFN ADE calculations within ConnectFlow. These are illustrative since they are constrained to a repository scale domain that does not include all the recharge and discharge locations. However, the calculations do include a realistic representation of the fractures at Forsmark. The DFN ADE simulations have been compared with equivalent ECPM calculations and equivalent DFN pathline calculations performed using the methodology used in SKB (2022b). A key result from this work is that flow paths may descend below repository depth prior to reaching a given location at repository depth. The salinity may then transiently increase as the simulation progresses, which will tend to increase the time taken for dilution to occur. This effect is not captured by the pathline-based method that assumes constant initial solute concentration throughout the fracture network.

Several recommendations for future work can be made. First, the DFN simulation mesh should be extended to include relevant recharge locations if the DFN ADE method is to be adopted for site-specific assessment. This mesh extension could be achieved either using a regional-scale DFN model or through a nested approach in which a repository-scale DFN is embedded within a regional-scale ECPM domain. Such combined models are under development within the ConnectFlow code.

Second, full coupling of the transport and flow calculations is desirable but of lower importance given the moderate differences between the coupled and tracer calculations presented in this report. Third, consideration should be given to whether two- or five-reference-water calculations are appropriate. The five-reference-water approach enables more detailed predictions of solute composition but introduces significant computational burden; the simpler two-reference-water method may be sufficient when only salinity is of interest.

Fourth, including chemical reactions may remove conservatism in repository water dilution calculations (Joyce et al. 2014; SKB 2022b). These can be included within ConnectFlow if warranted, recognising the additional complexity and computational cost involved.

Fifth, future development of pathline-based approaches could explore the incorporation of spatially variable initial salinity distributions and mixing/dispersion at fracture intersections, to further improve their representation of solute transport under repository conditions.

Finally, this work has focused on comparing different methodologies for calculating dilution and it was therefore deemed unnecessary to consider uncertainty within the fracture network. This uncertainty would likely need to be considered in a formal assessment, potentially by generating and simulating dilution for a range of different fracture realisations.

9 References

SKB's (Svensk Kärnbränslehantering AB) publications can be found at www.skb.com/publications. SKBdoc documents will be submitted upon request to document@skb.se.

Applegate D, Appleyard P, 2022. Capability for Hydrogeochemical Modelling within Discrete Fracture Networks. Energies 2022, 15(17), 6199; https://doi.org/10.3390/en15176199.

Bosson E, Gustafsson L-G, Sassner M, 2008. Numerical modelling of surface hydrology and near-surface hydrogeology at Forsmark. Site descriptive modelling, SDM-Site Forsmark. SKB R-08-09, Svensk Kärnbränslehantering AB.

Charlton S R, Parkhurst D L, 2011. Modules Based on the Geochemical Model PHREEQC for Use in Scripting and Programming Languages. Computers & Geosciences.

Follin S, 2008. Bedrock hydrogeology Forsmark. Site descriptive modelling, SDM-Site Forsmark. SKB R-08-95, Svensk Kärnbränslehantering AB.

Hartley L, Appleyard P, Baxter S, Hoek J, Joyce S, Mosley K (2018). Discrete fracture network modelling (Version 3) in support of Olkiluoto site description 2018. Posiva Working Report 2017-32, Posiva Oy.

Hedenström A, Sohlenius G, Strömgren M, Brydsten L, Nyman H, 2008. Depth and stratigraphy of regolith at Forsmark. Site descriptive modelling, SDM-Site Forsmark. SKB R-08-07. Svensk Kärnbränslehantering AB.

Jackson C P, Hoch, A R, Todman S, 2000. Self-consistency of a heterogeneous continuum porous medium representation of a fractured medium, Water Resources Research, 36, 189–202, https://doi.org/10.1029/1999WR900249, https://agupubs.onlinelibrary.wiley.com/doi/abs/10.1029/1999WR900249.

Joyce S, Simpson T, Hartley L, Applegate D, Hoek J, Jackson P, Swan D, Marsic N, Follin S, 2010a. Groundwater flow modelling of periods with temperate climate conditions – Forsmark. SKB R-09-20, Svensk Kärnbränslehantering AB.

Joyce S, Simpson T, Hartley L, Applegate D, Hoek J, Jackson P, Roberts D, Swan D, Gylling B, Marsic N, Rhén I, 2010b. Groundwater flow modelling of periods with temperate climate conditions – Laxemar. SKB R-09-24, Svensk Kärnbränslehantering AB.

Joyce S, Applegate D, Appleyard P, Gordon A, Heath T, Hunter F, Hoek J, Jackson P, Swan D, Woollard H, 2014a. Groundwater flow and reactive transport modelling in ConnectFlow. SKB R-14-19, Svensk Kärnbränslehantering AB.

Joyce S, Marsic N, Sidborn M, Woollard H, 2014b. Future evolution of groundwater composition at Forsmark during an extended temperate period. SKB R-14-26, Svensk Kärnbränslehantering AB.

Joyce S, Appleyard P, Gai G, Mather F, Williams T, 2021. Groundwater Flow and Transport Modelling in Support of the Safety Case for the Operating License Application. Posiva Working Report 2021-20.

Mahmoudzadeh B, Liu L, Moreno L, Neretnieks I, 2013. Solute transport in fractured rocks with stagnant water zone and rock matrix composed of different geological layers - model development and simulations. Water Resour. Res. 49,1709-1727.

Parkhurst D L, Appelo C, 1999. User's guide to PHREEQC (Version 2) - A computer program for speciation, batch-reaction, one-dimensional transport, and inverse geochemical calculations. U.S. Geological Survey Water-Resources Investigations Report 99–4259.

Posiva, 2021. Safety Case for the Operating Licence Application - Performance Assessment and Formulation of Scenarios (PAFOS). Posiva Report 2021-06, Posiva Oy.

Poteri A, 2009. Retention properties of the flow paths in fractured rock. Hydrogeology Journal. 17 pp. 1081-1092.

Poteri A, Nordman H, Pulkkanen V, Smith P, 2014. Radionuclide Transport in the Repository Near-Field and Far-Field. Posiva Report 2014-2, Posiva Oy.

Rhén I, Follin S, Hermanson J, 2003. Hydrological Site Descriptive Model – a strategy for its development during Site Investigations. SKB R-03-08, Svensk Kärnbärnslehantering AB.

Salas J, Gimeno J S, Auqué L, Molinero J, Gómez J, Juárez I, 2010. SR-Site – Hydrogeochemical evolution of the Forsmark site. SKB TR-10-58, Svensk Kärnbränslehantering AB.

Shahkarami P, 2024. Verification of a model for calculating the dilute water penetration in fractured rock – a MATLAB implementation. SKB R-24-15, Svensk Kärnbränslehantering AB.

SKB, 2008. Site description of Forsmark at completion of the site investigation phase. SDM-Site Forsmark. SKB TR-08-05, Svensk Kärnbränslehantering AB.

SKB, 2011. Long-term safety for the final repository for spent nuclear fuel at Forsmark Main report of the SR-Site project. SKB TR-11-01, Svensk Kärnbränslehantering AB.

SKB, 2022a. Post-closure safety for the final repository for spent nuclear fuel at Forsmark. Main report, PSAR version, SKB TR-21-01, Svensk Kärnbränslehantering AB.

SKB, 2022b. Post-closure safety for the final repository for spent nuclear fuel at Forsmark. Radionuclide transport report, PSAR version, SKB TR-21-07, Svensk Kärnbränslehantering AB.

Svensson, U, 1999. Representation of Fracture Networks as Grid Cell Conductivities, SKB TR-99-25, Svensk Kärnbränslehantering AB.

Vidstrand P, Follin S, Zugec N, 2010. Groundwater flow modelling of periods with periglacial and glacial climate conditions – SR-Site Forsmark. SKB R-09-21, Svensk Kärnbränslehantering AB.

Williams T, Sanglas J, Trinchero P, Gai G, Painter S L, Selroos J-O, 2021. Recovering the Effects of Subgrid Heterogeneity in Simulations of Radionuclide Transport Through Fractured Media. Front. Earth Sci. 8, 588.